Journal of Computational Physics 228 (2009) 2037–2062

Contents lists available at ScienceDirect

Journal of Computational Physics

journal homepage: www.elsevier.com/locate/jcp

The compressible hybrid RANS/LES formulation using an additive operator

Martín Sánchez-Rocha, Suresh Menon *

School of Aerospace Engineering, Georgia Institute of Technology, 270 Ferst Drive, Atlanta, GA 30332-0150, United States

ARTICLE INFO

Article history:
Received 13 October 2007
Received in revised form 26 May 2008
Accepted 17 November 2008
Available online 6 December 2008

PACS:
47.10.A–
47.10.Ad
47.27.E–
47.27.Em
47.27.Ep

Keywords:
Hybrid RANS/LES approach
Hybrid RANS/LES governing equations
Near-wall modeling
Turbulent boundary layer
LES

ABSTRACT

In this work, the compressible governing equations for the hybrid Reynolds-averaged/large-eddy simulations are formally derived by applying a hybrid filter to the Navier–Stokes equations. This filter is constructed by linearly combining the Reynolds-average (RANS) and large-eddy simulation (LES) operators with a continuous blending function. The derived hybrid equations include additional terms that represent the interactions between RANS and LES formulations. The relevance of these terms is investigated in flat-plate turbulent boundary layer simulations and indicate that these additional terms play a fundamental role in compensating for the turbulence that is neither modeled nor resolved in the transition region between RANS and LES. Results also show that when the additional terms are included, the calculations are not very sensitive to the blending function implemented in the hybrid filter. In the contrary, when these terms are neglected and a step function is implemented in the hybrid filter, nonphysical discontinuities are predicted in the flow statistics.

© 2008 Elsevier Inc. All rights reserved.

1. Introduction

Hybrid Reynolds-averaged/large eddy simulation is a relatively new concept aimed at making possible complex high Reynolds number turbulence simulations for engineering applications. It brings together two currently employed turbulence modeling approaches: Reynolds-average Navier–Stokes (RANS) and large-eddy simulation (LES), and is motivated by the inability of RANS models to predict complex unsteady flows [1], and the prohibitively high cost of LES in high Reynolds number wall-resolved simulations [2]. In general, the hybrid RANS/LES formulation can be interpreted as a model intended to reduce the high cost of LES simulations. Although the idea of using RANS as a near-wall model for LES simulations can be found in the early work of Schumann [3], hybrid RANS/LES models were not seriously consider until Spalart et al. [4] and Speziale [5] explicitly introduced practical hybrid approaches.

In the approach of Spalart et al. [4], the Spalart–Allmaras RANS model [6] is modified to reduce the amount of turbulence viscosity provided in regions of massive flow separation, while in regions of attach flow, RANS level of the modeled turbulent viscosity is provided. This model was named detached eddy simulation (DES), implying that it should be used in flows where massive flow separation controls the unsteady flow dynamics. DES has been successfully applied to a broad range of problems spanning complex engineering applications to canonical flows studies [1,7–12]. However, as any other model, DES has advantages and disadvantages that compromise the accuracy of its predictions [9,13,14]. A characteristic limitation of DES is

* Corresponding author. Tel.: +1 404 894 9126; fax: +1 404 894 2760.
E-mail addresses: martin_sanchez-rocha@gatech.edu (M. Sánchez-Rocha), suresh.menon@ae.gatech.edu (S. Menon).

0021-9991/$ - see front matter © 2008 Elsevier Inc. All rights reserved.
doi:10.1016/j.jcp.2008.11.021

its transition from RANS to LES, which is grid controlled. Here, grid refinements made to improve the description of the geometry can dramatically interfere with the model transition, inducing inaccurate predictions. A correction for this latent source of error have been proposed in a new version of this model [15], which still remains to be carefully explored.

A different hybrid RANS/LES approach was introduced by Speziale [5]. He proposed a formulation capable of bridging direct numerical simulations (DNS) with RANS modeling with LES in-between, in what he referred to as very-large eddy simulations (VLES). In this approach, the subgrid stress tensor (τ_{ij}^s) is computed by rescaling the RANS Reynolds stress tensor (τ_{ij}^R) as

$$\tau_{ij}^s = \alpha \tau_{ij}^R, \quad \alpha = [1 - \exp(-\beta \Delta/\eta)]^n, \tag{1.1}$$

depending on whether the grid is fine enough to resolve turbulence scales. Speziale only suggested the form of the rescaling factor (α) as function of the grid resolution (Δ) and the Kolmolgorov length scale (η); the constants β and n were left unspecified. Other researchers proposed different formulations to implement this approach. Some examples are the limited numerical scales (LNS) model of Batten et al. [16], the partially resolved numerical simulation of Liu et al. [17], the renormalization group model of Delanghe et al. [18], the partially averaged Navier–Stokes model of Girimaji [19], and the model of Befeno and Schiestel [20]. All these approaches have been applied in both simple and complex flows demonstrating the potential of Speziale's original idea. It is important to highlight that this formulation is not restricted to act as a near-wall model for LES, since the transition can occur in any flow region where the grid resolution is fine enough to sustain LES or even DNS simulations.

Recently, other hybrid formulations have appeared in the literature, such as the zonal [2,21–29] and the blended [30–35] approaches. In the zonal approach, RANS modeling is implemented as a near-wall model for LES simulations by solving both models in different flow regions (here, the matching plane or interface between the models is specified arbitrarily). Davidson and Peng [36] and Tucker and Davidson [23] combined the RANS $k-\omega$ and $k-l$ models with a one-equation model for the subgrid kinetic energy (k^{sgs}) to simulate the turbulent flow over a channel, over a ribbed channel, and over a 3 D hill. Their results showed marked discontinuities in the flow statistics and in the turbulence variables independently of the location of the matching plane. Hamba [22,29] conducted zonal simulations of channel flows and observed unphysical mismatches in the flow statistics close to the model interface. He demonstrated that even when LES is conducted in the near-wall region and RANS in the core of the channel, the zonal approach still predicted unphysical results. He proposed an additional filtering approach at the model's interface to correct the errors observed in the flow statistics.

Temmerman et al. [27] implemented the RANS $k-\epsilon$ and the $k-l$ models together with the Smagorinsky LES model [37] to conduct channel and hill flow simulations. They proposed a matching criterion at the model's interface to control the amount of modeled turbulent viscosity to reduce the discontinuities predicted in the flow statistics. Davidson and Dahlström [26] proposed the inclusion of turbulence fluctuations at the interface to reduce the discrepancies observed in previous channel simulations. Their approach improved zonal predictions for channel flows, however, it required a precursor DNS simulation. Davidson and Billson [28] proposed the inclusion of synthesized turbulence at the interface, and evaluated isotropic and anisotropic fluctuations in channel flows. Overall, this approach improved the predicted statistics at the model interface. Similar stochastic forcing approaches have been also proposed in the DES framework by Piomelli et al. [8] and Keating and Piomelli [11], and in LNS by Batten et al. [16]. Thus, it appears from these studies that the zonal approach when used as a near-wall model has the potential to reduce the high cost of wall-resolved LES simulations [2]. Nevertheless, this approach has to be carefully implemented to avoid unphysical predictions when attached flow conditions are simulated. Additionally, this approach (as proposed so far) lacks a general criterion to specify the location of the model's interface. This is a critical issue since (at least, for the models discussed above) the location of the interface can impact the predictions significantly.

In addition to the near wall model approach the zonal RANS/LES model has been also applied to provide inflow conditions to LES simulations. Georgiadis et al. [21] conducted LES simulations of a compressible mixing layer where the flow upstream of the splitter was simulated with RANS to reduce the cost of the simulation. A similar coupling strategy by Schluter et al. [24], was employed for simulations of gas turbine configurations, where the compressor was simulated with RANS and the combustor chamber with LES. Although this strategy is still considered a zonal hybrid RANS/LES approach, the coupling between formulations is only through boundary conditions limiting the interaction among the two formulations.

In the blended approach, a hybrid model is constructed by smoothly combining compatible RANS and LES model equations. This formulation is similar to the zonal approach since the RANS is used as a near-wall model for LES; however, the transition between models occurs smoothly in a well-defined region. Baurle et al. [32] proposed that any trusted RANS and LES models containing equations for the turbulent kinetic energy (k) and subgrid kinetic energy (k^{sgs}) could be smoothly combined to design a single hybrid model equation. They combined a two-equation RANS $k-\omega$ model and a one-equation LES model for k^{sgs} to conduct simulations of cavity flows. Xiao et al. [31,33] and Fan et al. [34] implemented RANS $k-\zeta$ and RANS-SST $k-\omega$ models with a LES one-equation for k^{sgs} to simulate the flow over a compression ramp. In general, the performance of these models is also encouraging. Nevertheless, significant amount of work has still to be conducted to evaluate and quantify the effect of the blending function and the turbulence models used in the simulations, even when some of these issues have been already investigated in the past [31,33]. In principle, there is no reason why only models containing equations for k and k^{sgs} should be used to construct hybrid blended models. The hybrid blended approach should be presented in a general form independent of the types of RANS and LES models employed.

In general, very few researchers have developed a theoretical formulation for the hybrid RANS/LES approach [38–41]. In combining RANS with LES models, most approaches ignore the fundamental differences between the RANS and the LES

formulations [8,42]. Thus, most reported approaches become engineering methods driven by practical necessity for simulating high Reynolds number flows with available computing resources. There have been, however, some theoretical attempts to develop a general framework for the hybrid approach. For example, Germano [39] demonstrated that the governing equations derived by applying a hybrid filter (created by smoothly combining the RANS and the LES operators) include new hybrid terms that should not be neglected. His formal derivation (albeit, restricted to incompressible flows) indicates that hybrid formulations cannot rely only on the capability of the turbulence models to switch from RANS to LES. However, he did not apply this approach to any flow problem.

In this paper, we extend Germano [39] theoretical formulation to compressible flow by deriving the unsteady, compressible hybrid RANS/LES N–S equations. The importance of the hybrid terms in the hybrid formulation is assessed by conducting LES and hybrid RANS/LES simulations for an attached turbulent boundary layer over a flat-plate. Additionally, the effect of the blending function used in the hybrid filter is analyzed. Finally, the effect of grid resolution in the hybrid simulations is also investigated.

2. Formulation

The properties of additive filters, constructed by blending two or more independent operators in the framework of computational fluid dynamics were formally described by Germano [39]. In particular, he defined a hybrid RANS/LES filter by blending the RANS statistical operator and the LES filter operator and went on to derive the hybrid incompressible N–S equations. The resulting differential equations depend explicitly on the hybrid variables, on the statistically operated, and on the filtered quantities increasing the number of independent variables. To close the equations, Germano introduced a simple reconstruction procedure, which in theory allows the calculation of the statistical and the filtered field from the hybrid variables. Although Germano did not present any numerical results to demonstrate the feasibility of the formulation, we consider that the procedure is fundamentally correct and extend it here to compressible flows.

2.1. Operators

In order to clearly derive the compressible hybrid RANS/LES governing equations a new symbology is introduced to avoid confusion between formulations. In this paper, RANS, LES, and hybrid operated on a dummy variable (ϕ) are identified as follows:

RANS variables:

$$\dot{\bar{\phi}},\ \phi^{\dot{\prime}},\ \dot{\tilde{\phi}},\ \phi^{\dot{\prime\prime}}. \tag{2.1}$$

LES variables:

$$\ddot{\bar{\phi}},\ \phi^{\ddot{\prime}},\ \ddot{\tilde{\phi}},\ \phi^{\ddot{\prime\prime}}. \tag{2.2}$$

Hybrid variables:

$$\bar{\phi},\ \phi',\ \tilde{\phi},\ \phi''. \tag{2.3}$$

We define the RANS operator as a statistical ensemble average together with its Favre (density weighted) representation as

$$\dot{\bar{\phi}}(x_i,t) = \lim_{N\to\infty}\frac{1}{N}\sum_{k=1}^{N}\phi^{(k)}(x_i,t), \tag{2.4}$$

$$\dot{\tilde{\phi}}(x_i,t) = \frac{\dot{\overline{\rho\phi}}}{\dot{\bar{\rho}}}. \tag{2.5}$$

Here, ρ is density, x_i is the space vector, t is time, and N represent the number of realization/experiments conducted for $\phi^{(k)}$, which is a function of time and space. For RANS, the separation of scales is achieved by constructing the unsteady variable (ϕ) either by using the statistical mean ($\dot{\bar{\phi}}$) and the unsteady fluctuation ($\phi^{\dot{\prime}}$) or the Favre mean ($\dot{\tilde{\phi}}$) and the unsteady Favre fluctuation ($\phi^{\dot{\prime\prime}}$). In this study, it is assumed that the RANS operator satisfies the ergodic hypothesis and the Reynolds rules of averaging [43]. Thus,

$$\dot{\overline{\phi+\psi}} = \dot{\bar{\phi}} + \dot{\bar{\psi}}, \tag{2.6a}$$

$$\dot{\bar{\alpha}} = \alpha, \tag{2.6b}$$

$$\dot{\overline{\alpha\phi}} = \alpha\dot{\bar{\phi}}, \tag{2.6c}$$

$$\dot{\overline{\phi\dot{\bar{\psi}}}} = \dot{\bar{\phi}}\dot{\bar{\psi}}, \tag{2.6d}$$

$$\phi^{\dot{\prime}} = \phi - \dot{\bar{\phi}}, \quad \phi^{\dot{\prime\prime}} = \phi - \dot{\tilde{\phi}}, \tag{2.6e}$$

$$\dot{\bar{\phi}} = \dot{\bar{\phi}}, \quad \dot{\tilde{\phi}} = \dot{\tilde{\phi}}, \tag{2.6f}$$

$$\dot{\overline{\phi'}} = 0, \quad \dot{\overline{\phi''}} \neq 0, \tag{2.6g}$$

$$\dot{\overline{\rho\phi'}} \neq 0, \quad \dot{\overline{\rho\phi''}} = 0. \tag{2.6h}$$

Here, ψ and α are another dummy variable and a constant, respectively.

For the LES formulation, a low-pass space filter is implemented to perform scale separation. In general, the LES operator and its Favre representation can be defined as

$$\ddot{\bar{\phi}}(x_i,t) = \int_{-\infty}^{+\infty} G(x_i - r_i, \Delta)\phi(r_i,t)dr_i, \tag{2.7}$$

$$\ddot{\tilde{\phi}}(x_i,t) = \frac{\ddot{\overline{\rho\phi}}}{\ddot{\bar{\rho}}}, \tag{2.8}$$

where $\ddot{\bar{\phi}}$ and $\ddot{\tilde{\phi}}$ represent the filtered and the Favre filtered variables, respectively, and G and Δ represent the filter kernel and filter width, respectively.

Similar to the RANS formulation, the unsteady variable (ϕ) is constructed, in the LES formulation, by using the filtered variables ($\phi = \ddot{\bar{\phi}} + \phi^{\ddot{\prime}}$) and the Favre filtered representation ($\phi = \ddot{\tilde{\phi}} + \phi^{\ddot{\prime\prime}}$). However, unlike the RANS operator, which is generic, the LES operator requires a kernel function (G) and filter width (Δ) that need to be defined, thus constraining the generality of the LES operator. In the literature, different LES filters have been proposed spanning explicit and implicit (grid) filters [40]. Nevertheless, their mathematical properties differ and general properties cannot be easily stated. Here, we only mention that for most LES filters [40,44] not all the Reynolds rules of averaging apply. The properties that are most commonly applicable are

$$\ddot{\overline{\phi + \psi}} = \ddot{\bar{\phi}} + \ddot{\bar{\psi}}, \tag{2.9a}$$

$$\ddot{\bar{\alpha}} = \alpha, \tag{2.9b}$$

$$\ddot{\overline{\alpha\phi}} = \alpha\ddot{\bar{\phi}}, \tag{2.9c}$$

$$\ddot{\overline{\phi\psi}} \neq \ddot{\bar{\phi}}\ddot{\bar{\psi}}, \tag{2.9d}$$

$$\phi^{\ddot{\prime}} = \phi - \ddot{\bar{\phi}}, \quad \phi^{\ddot{\prime\prime}} = \phi - \ddot{\tilde{\phi}}, \tag{2.9e}$$

$$\ddot{\bar{\phi}} \neq \ddot{\bar{\phi}}, \quad \ddot{\tilde{\phi}} \neq \ddot{\bar{\phi}}, \tag{2.9f}$$

$$\ddot{\overline{\phi'}} \neq 0, \quad \ddot{\overline{\phi''}} \neq 0, \tag{2.9g}$$

$$\ddot{\overline{\rho\phi'}} \neq 0, \quad \ddot{\overline{\rho\phi''}} \neq 0, \tag{2.9h}$$

where $\phi^{\ddot{\prime}}$ and $\phi^{\ddot{\prime\prime}}$ represent the subgrid fluctuation and the subgrid density-weighted fluctuation, respectively. In this study, we consider a generic low-pass LES filter with the only restrictions that it commutes with differentiation and with the statistical operator [39]. That is,

$$\frac{\ddot{\overline{\partial\phi}}}{\partial x_i} = \frac{\partial\ddot{\bar{\phi}}}{\partial x_i}, \tag{2.10}$$

$$\dot{\bar{\phi}} = \ddot{\bar{\phi}} = \dot{\bar{\phi}}. \tag{2.11}$$

Having defined the RANS and the LES operators, a hybrid additive operator and its Favre representation can be constructed by combining Eqs. (2.4) and (2.7) with a blending function

$$\bar{\phi}(x_i,t) = \mathcal{F}\dot{\bar{\phi}}(x_i,t) + (1-\mathcal{F})\ddot{\bar{\phi}}(x_i,t) \tag{2.12}$$

$$\tilde{\phi}(x_i,t) = \frac{\overline{\rho\phi}}{\bar{\rho}}. \tag{2.13}$$

Here, $\mathcal{F}$ is a normalized function that in general, depends on time and space. It is defined as $\mathcal{F} : \{ (\|x_i\|,t) \in [0,\infty) \to \mathcal{F}(x_i,t) \in [0,1] \}$. Furthermore, it must have continuous derivatives to at least second-order in space and first-order in time, i.e., $\mathcal{F}(x_i,t)$ is a $C^2(x_i)$ and $C^1(t)$ function (this will be evident when the hybrid equations are derived). Under this hybrid definition, Eq. (2.12) recovers RANS and LES variables when $\mathcal{F} = 1$ and $\mathcal{F} = 0$, respectively. Similar to RANS and LES, the unsteady variable (ϕ) can be constructed using the hybrid variables with the standard decomposition:

$$\phi = \bar{\phi} + \phi', \quad \phi = \tilde{\phi} + \phi''. \tag{2.14}$$

Here, the hybrid fluctuations can be easily shown to be related to the RANS and LES fluctuations as

$$\phi' = \mathcal{F}\phi^{\dot{'}} + (1-\mathcal{F})\phi^{\ddot{'}} \tag{2.15}$$

and

$$\phi'' = \mathcal{F}\frac{\dot{\bar{\rho}}}{\bar{\rho}}\phi^{\dot{''}} + (1-\mathcal{F})\frac{\ddot{\bar{\rho}}}{\bar{\rho}}\phi^{\ddot{''}}. \tag{2.16}$$

It can also be shown that, in general, the hybrid filter equation (2.12) does not commute with differentiation and does not satisfy all the Reynolds rules of averaging regardless the properties of the constitutive operators. Thus,

$$\overline{\frac{\partial\phi}{\partial x_i}} = \frac{\partial\bar{\phi}}{\partial x_i} + \frac{\partial\mathcal{F}}{\partial x_i}(\ddot{\bar{\phi}} - \dot{\bar{\phi}}), \tag{2.17a}$$

$$\overline{\frac{\partial\phi}{\partial t}} = \frac{\partial\bar{\phi}}{\partial t} + \frac{\partial\mathcal{F}}{\partial t}(\ddot{\bar{\phi}} - \dot{\bar{\phi}}), \tag{2.17b}$$

$$\overline{\phi+\psi} = \bar{\phi} + \bar{\psi}, \tag{2.18a}$$

$$\bar{\alpha} = \alpha, \tag{2.18b}$$

$$\overline{\alpha\phi} = \alpha\bar{\phi}, \tag{2.18c}$$

$$\overline{\phi\bar{\psi}} \neq \bar{\phi}\bar{\psi}, \tag{2.18d}$$

$$\overline{\bar{\phi}} \neq \bar{\phi}, \quad \widetilde{\bar{\phi}} \neq \tilde{\phi}, \tag{2.18e}$$

$$\overline{\phi'} \neq 0, \quad \overline{\phi''} \neq 0, \tag{2.18f}$$

$$\overline{\rho\phi'} \neq 0, \quad \overline{\rho\phi''} \neq 0, \tag{2.18g}$$

since

$$\overline{\bar{\phi}} = (2-\mathcal{F})\mathcal{F}\dot{\bar{\phi}} + (1-\mathcal{F})^2\ddot{\bar{\phi}}. \tag{2.19}$$

Eqs. (2.17) and (2.19) indicate that the hybrid filter does not commute with differentiation, and the application of the hybrid operator on the hybrid variable does not recover the same hybrid variable, i.e., $\overline{\bar{\phi}} \neq \bar{\phi}$. These are general properties of this hybrid operator, and do not depend on the constitutive operators.

The last relevant property of the hybrid operator is related to its ability to reconstruct the RANS and the LES variables if the hybrid field is known. Germano [39] showed that by applying Eq. (2.4) in Eq. (2.12) and invoking Eq. (2.11), the RANS variable can be calculated directly from the hybrid variable as

$$\dot{\phi} = \dot{\bar{\phi}}. \tag{2.20}$$

Once the RANS field is known, the LES variable can be obtained by substituting Eq. (2.20) in Eq. (2.12)

$$\ddot{\phi} = \frac{\bar{\phi} - \mathcal{F}\dot{\bar{\phi}}}{1-\mathcal{F}}. \tag{2.21}$$

To extend Germano's original incompressible formulation to compressible flow, the governing equations have to be derived using the generalized second-order central-moments [44]. This allows us a better representation of the unclosed terms that appears when we apply the operator in the nonlinear terms. This way, the final equations are invariant with respect to the operators employed. For the compressible formulation, the generalized second-order central-moments are defined as

$$\dot{\tau}(a,b) = \dot{\rho}(\dot{\widetilde{ab}} - \dot{\tilde{a}}\dot{\tilde{b}}), \quad \dot{\chi}(a,b) = \dot{\overline{ab}} - \dot{\tilde{a}}\dot{\bar{b}}, \quad \dot{\zeta}(a,b) = \dot{\overline{ab}} - \dot{\tilde{a}}\dot{\tilde{b}}, \tag{2.22}$$

$$\ddot{\tau}(a,b) = \ddot{\rho}(\ddot{\widetilde{ab}} - \ddot{\tilde{a}}\ddot{\tilde{b}}), \quad \ddot{\chi}(a,b) = \ddot{\overline{ab}} - \ddot{\tilde{a}}\ddot{\bar{b}}, \quad \ddot{\zeta}(a,b) = \ddot{\overline{ab}} - \ddot{\tilde{a}}\ddot{\tilde{b}}, \tag{2.23}$$

$$\bar{\tau}(a,b) = \bar{\rho}(\widetilde{ab} - \tilde{a}\tilde{b}), \quad \bar{\chi}(a,b) = \overline{ab} - \tilde{a}\bar{b}, \quad \bar{\zeta}(a,b) = \overline{ab} - \tilde{a}\tilde{b}. \tag{2.24}$$

Here a and b are dummy variables and τ, χ, and ζ represent, the compressible operators required by the RANS, the LES, and the hybrid formulation. It is important to highlight that τ and ζ are symmetric operators while χ is not. Additionally, both χ and ζ operators are required to account for the additional nonlinear terms present in the energy equation, and therefore they do not appear in Germano's [39] incompressible formulation. By substituting Eqs. (2.12) and (2.13) in Eq. (2.24) the dependency of the hybrid central-moments on the RANS and LES variables can be shown to be

$$\begin{aligned}\bar{\tau}(a,b) = {} & \mathcal{F}\dot{\tau}(a,b) + (1-\mathcal{F})\ddot{\tau}(a,b) + \bar{\rho}\left[\mathcal{F}\left(1-\mathcal{F}\frac{\dot{\bar{\rho}}}{\bar{\rho}}\right)\frac{\dot{\bar{\rho}}}{\bar{\rho}}\dot{\tilde{a}}\dot{\tilde{b}} - \mathcal{F}(1-\mathcal{F})\frac{\dot{\bar{\rho}}\ddot{\bar{\rho}}}{\bar{\rho}^2}\dot{\tilde{a}}\ddot{\tilde{b}}\right] \\ & + \bar{\rho}\left[(1-\mathcal{F})\left(1-(1-\mathcal{F})\frac{\ddot{\bar{\rho}}}{\bar{\rho}}\right)\frac{\ddot{\bar{\rho}}}{\bar{\rho}}\ddot{\tilde{a}}\ddot{\tilde{b}} - \mathcal{F}(1-\mathcal{F})\frac{\dot{\bar{\rho}}\ddot{\bar{\rho}}}{\bar{\rho}^2}\ddot{\tilde{a}}\dot{\tilde{b}}\right],\end{aligned} \tag{2.25}$$

$$\bar{\chi}(a,b) = \mathcal{F}\dot{\chi}(a,b) + (1-\mathcal{F})\ddot{\chi}(a,b) + \left[\mathcal{F}\left(1-\mathcal{F}\frac{\dot{\bar{\rho}}}{\bar{\rho}}\right)\dot{\tilde{a}}\dot{\tilde{b}} - \mathcal{F}(1-\mathcal{F})\frac{\dot{\bar{\rho}}}{\bar{\rho}}\dot{\tilde{a}}\ddot{\tilde{b}}\right] + \left[(1-\mathcal{F})\left(1-(1-\mathcal{F})\frac{\ddot{\bar{\rho}}}{\bar{\rho}}\right)\ddot{\tilde{a}}\ddot{\tilde{b}} - \mathcal{F}(1-\mathcal{F})\frac{\ddot{\bar{\rho}}}{\bar{\rho}}\ddot{\tilde{a}}\dot{\tilde{b}}\right], \tag{2.26}$$

$$\bar{\zeta}(a,b) = \mathcal{F}\dot{\zeta}(a,b) + (1-\mathcal{F})\ddot{\zeta}(a,b) + \left[\mathcal{F}\left(1-\mathcal{F}\frac{\dot{\bar{\rho}}^2}{\bar{\rho}^2}\right)\dot{\tilde{a}}\dot{\tilde{b}} - \mathcal{F}(1-\mathcal{F})\frac{\dot{\bar{\rho}}\ddot{\bar{\rho}}}{\bar{\rho}^2}\dot{\tilde{a}}\ddot{\tilde{b}}\right] + \left[(1-\mathcal{F})\left(1-(1-\mathcal{F})\frac{\ddot{\bar{\rho}}^2}{\bar{\rho}^2}\right)\ddot{\tilde{a}}\ddot{\tilde{b}} - \mathcal{F}(1-\mathcal{F})\frac{\dot{\bar{\rho}}\ddot{\bar{\rho}}}{\bar{\rho}^2}\ddot{\tilde{a}}\dot{\tilde{b}}\right]. \tag{2.27}$$

It is trivial to show that these equations recover RANS and LES central moments when $\mathcal{F}=1$ and $\mathcal{F}=0$, respectively. Using the above operator, the hybrid Reynolds stress tensor is constructed by operating Eq. (2.25) on u_i and u_j:

$$\bar{\tau}(u_i,u_j) = \mathcal{F}\dot{\bar{\rho}}(\dot{\widetilde{u_iu_j}} - \dot{\tilde{u}}_i\dot{\tilde{u}}_j) + (1-\mathcal{F})\ddot{\bar{\rho}}(\ddot{\widetilde{u_iu_j}} - \ddot{\tilde{u}}_i\ddot{\tilde{u}}_j) + \bar{\rho}\left[\mathcal{F}\left(1-\mathcal{F}\frac{\dot{\bar{\rho}}}{\bar{\rho}}\right)\frac{\dot{\bar{\rho}}}{\bar{\rho}}\dot{\tilde{u}}_i\dot{\tilde{u}}_j - \mathcal{F}(1-\mathcal{F})\frac{\dot{\bar{\rho}}\ddot{\bar{\rho}}}{\bar{\rho}^2}\dot{\tilde{u}}_i\ddot{\tilde{u}}_j\right] + \bar{\rho}\left[(1-\mathcal{F})\left(1-(1-\mathcal{F})\frac{\ddot{\bar{\rho}}}{\bar{\rho}}\right)\frac{\ddot{\bar{\rho}}}{\bar{\rho}}\ddot{\tilde{u}}_i\ddot{\tilde{u}}_j - \mathcal{F}(1-\mathcal{F})\frac{\dot{\bar{\rho}}\ddot{\bar{\rho}}}{\bar{\rho}^2}\ddot{\tilde{u}}_i\dot{\tilde{u}}_j\right]. \tag{2.28}$$

It is clear that the compressible generic central-moments in their explicit form include density ratios induced by the Favre formulation that do not appear in the incompressible formulation of Germano [39]. However, it is easy to show (see Appendix) that for incompressible flow equation (2.28) reduces to the incompressible hybrid Reynolds stress tensor derived by Germano.

2.2. Compressible hybrid Navier–Stokes equations

Having established the required hybrid operators, Eqs. (2.12)–(2.27) we apply them to the unsteady compressible N–S equations for a calorically perfect gas and Newtonian fluid. The original equations are

$$\frac{\partial\rho}{\partial t} + \frac{\partial}{\partial x_j}(\rho u_j) = 0, \tag{2.29}$$

$$\frac{\partial\rho u_i}{\partial t} + \frac{\partial}{\partial x_j}(\rho u_i u_j) = \frac{\partial}{\partial x_j}(-p\delta_{ij} + \tau_{ij}), \tag{2.30}$$

$$\frac{\partial\rho E}{\partial t} + \frac{\partial}{\partial x_j}(\rho u_j E) = \frac{\partial}{\partial x_j}\left(\kappa\frac{\partial T}{\partial x_j} + (-p\delta_{ij} + \tau_{ij})u_i\right), \tag{2.31}$$

$$p = \rho RT, \tag{2.32}$$

$$\rho E = \rho C_v T + \frac{\rho}{2}u_k u_k, \tag{2.33}$$

$$\tau_{ij} = 2\mu\left(S_{ij} - \frac{1}{3}S_{kk}\delta_{ij}\right), \quad S_{ij} = \frac{1}{2}\left(\frac{\partial u_i}{\partial x_j} + \frac{\partial u_j}{\partial x_i}\right). \tag{2.34}$$

Here, u_i is velocity, p is pressure, μ is the molecular viscosity, E is the total energy, T is temperature, R is the gas constant, C_v is the specific heat at constant volume, κ is the heat conductivity, and δ_{ij} is the Kronecker delta. After some algebraic manipulations, the hybrid compressible N–S equations can be shown to be

$$\frac{\partial\bar{\rho}}{\partial t} + \frac{\partial}{\partial x_j}(\bar{\rho}\tilde{u}_j) = \frac{\partial\mathcal{F}}{\partial x_j}[\dot{\bar{\rho}}\dot{\tilde{u}}_j - \ddot{\bar{\rho}}\ddot{\tilde{u}}_j] + \frac{\partial\mathcal{F}}{\partial t}[\dot{\bar{\rho}} - \ddot{\bar{\rho}}], \tag{2.35}$$

$$\frac{\partial\bar{\rho}\tilde{u}_i}{\partial t} + \frac{\partial}{\partial x_j}(\bar{\rho}\tilde{u}_i\tilde{u}_j + \bar{p}\delta_{ij} - \tilde{\tau}_{ij} + \bar{\tau}(u_i,u_j)) = \frac{\partial\mathcal{F}}{\partial x_j}[\dot{\bar{\rho}}\dot{\tilde{u}}_i\dot{\tilde{u}}_j - \ddot{\bar{\rho}}\ddot{\tilde{u}}_i\ddot{\tilde{u}}_j + \dot{\tilde{\tau}}(u_i,u_j) - \ddot{\tilde{\tau}}(u_i,u_j) + (\dot{\bar{p}} - \ddot{\bar{p}})\delta_{ij} - (\dot{\tilde{\tau}}_{ij} - \ddot{\tilde{\tau}}_{ij})] - \frac{\partial}{\partial x_j}\left\{\frac{\partial\mathcal{F}}{\partial x_j}(\dot{\bar{\mu}}\dot{\tilde{u}}_i - \ddot{\bar{\mu}}\ddot{\tilde{u}}_i) + \frac{\partial\mathcal{F}}{\partial x_i}(\dot{\bar{\mu}}\dot{\tilde{u}}_j - \ddot{\bar{\mu}}\ddot{\tilde{u}}_j) - \frac{2}{3}\frac{\partial\mathcal{F}}{\partial x_k}(\dot{\bar{\mu}}\dot{\tilde{u}}_k - \ddot{\bar{\mu}}\ddot{\tilde{u}}_k)\delta_{ij}\right\} + \frac{\partial\mathcal{F}}{\partial t}[\dot{\bar{\rho}}\dot{\tilde{u}}_i - \ddot{\bar{\rho}}\ddot{\tilde{u}}_i], \tag{2.36}$$

$$\frac{\partial\bar{\rho}\widetilde{E}}{\partial t} + \frac{\partial}{\partial x_j}\left(\bar{\rho}\widetilde{E}\tilde{u}_j + \bar{p}\tilde{u}_j - \bar{\kappa}\frac{\partial\widetilde{T}}{\partial x_j} - \tilde{\tau}_{ij}\tilde{u}_i + \bar{\tau}(E,u_j) + \bar{\chi}(u_j,p) - \bar{\chi}\left(\frac{\partial T}{\partial x_j},\kappa\right) - \bar{\zeta}(\tau_{ij},u_i)\right) = \frac{\partial\mathcal{F}}{\partial x_j}\left\{\dot{\bar{\rho}}\dot{\tilde{u}}_j\dot{\widetilde{E}} - \ddot{\bar{\rho}}\ddot{\tilde{u}}_j\ddot{\widetilde{E}} + \dot{\tilde{\tau}}(E,u_j) - \ddot{\tilde{\tau}}(E,u_j) + \dot{\tilde{u}}_j\dot{\bar{p}} - \ddot{\tilde{u}}_j\ddot{\bar{p}} + \dot{\bar{\chi}}(u_j,p) - \ddot{\bar{\chi}}(u_j,p) - \left(\dot{\bar{\kappa}}\frac{\partial\dot{\widetilde{T}}}{\partial x_j} - \ddot{\bar{\kappa}}\frac{\partial\ddot{\widetilde{T}}}{\partial x_j} + \dot{\bar{\chi}}\left(\frac{\partial T}{\partial x_j},\kappa\right) - \ddot{\bar{\chi}}\left(\frac{\partial T}{\partial x_j},\kappa\right)\right) - \left(\dot{\tilde{\tau}}_{ij}\dot{\tilde{u}}_i - \ddot{\tilde{\tau}}_{ij}\ddot{\tilde{u}}_i + \dot{\bar{\zeta}}(\tau_{ij},u_i) - \ddot{\bar{\zeta}}(\tau_{ij},u_i)\right)\right\} + \frac{\partial\mathcal{F}}{\partial t}[\dot{\bar{\rho}}\dot{\widetilde{E}} - \ddot{\bar{\rho}}\ddot{\widetilde{E}}] \tag{2.37}$$

with the pressure, shear stress tensor, and total energy defined as

$$\bar{p} = \bar{\rho} R \widetilde{T}, \tag{2.38}$$

$$\tilde{\tau}_{ij} = 2\bar{\mu}\left(\widetilde{S}_{ij} - \frac{1}{3}\widetilde{S}_{kk}\delta_{ij}\right), \quad \widetilde{S}_{ij} = \frac{1}{2}\left(\frac{\partial \tilde{u}_i}{\partial x_j} + \frac{\partial \tilde{u}_j}{\partial x_i}\right), \tag{2.39a}$$

$$\dot{\tau}_{ij} = 2\dot{\mu}\left(\dot{\widetilde{S}}_{ij} - \frac{1}{3}\dot{\widetilde{S}}_{kk}\delta_{ij}\right), \quad \dot{\widetilde{S}}_{ij} = \frac{1}{2}\left(\frac{\partial \dot{\tilde{u}}_i}{\partial x_j} + \frac{\partial \dot{\tilde{u}}_j}{\partial x_i}\right), \tag{2.39b}$$

$$\ddot{\tau}_{ij} = 2\ddot{\mu}\left(\ddot{\widetilde{S}}_{ij} - \frac{1}{3}\ddot{\widetilde{S}}_{kk}\delta_{ij}\right), \quad \ddot{\widetilde{S}}_{ij} = \frac{1}{2}\left(\frac{\partial \ddot{\tilde{u}}_i}{\partial x_j} + \frac{\partial \ddot{\tilde{u}}_j}{\partial x_i}\right), \tag{2.39c}$$

$$\bar{\rho}\widetilde{E} = \bar{\rho} C_v \widetilde{T} + \frac{\bar{\rho}}{2}\tilde{u}_i\tilde{u}_i + \frac{1}{2}\bar{\tau}(u_i, u_i), \tag{2.40a}$$

$$\dot{\bar{\rho}}\dot{\widetilde{E}} = \dot{\bar{\rho}} C_v \dot{\widetilde{T}} + \frac{\dot{\bar{\rho}}}{2}\dot{\tilde{u}}_i\dot{\tilde{u}}_i + \frac{1}{2}\dot{\bar{\tau}}(u_i, u_i) \tag{2.40b}$$

$$\ddot{\bar{\rho}}\ddot{\widetilde{E}} = \ddot{\bar{\rho}} C_v \ddot{\widetilde{T}} + \frac{\ddot{\bar{\rho}}}{2}\ddot{\tilde{u}}_i\ddot{\tilde{u}}_i + \frac{1}{2}\ddot{\bar{\tau}}(u_i, u_i). \tag{2.40c}$$

As expected, the application of the hybrid operator to the N–S equations results in unclosed terms that need to be modeled. Furthermore, the hybrid operator introduces new terms into the final equations. These terms are

$$\sigma_\rho = \frac{\partial \mathcal{F}}{\partial x_j}[\dot{\bar{\rho}}\dot{\tilde{u}}_j - \ddot{\bar{\rho}}\ddot{\tilde{u}}_j] + \frac{\partial \mathcal{F}}{\partial t}[\dot{\bar{\rho}} - \ddot{\bar{\rho}}] \tag{2.41}$$

$$\begin{aligned}\sigma_{\rho u_i} = {} & \frac{\partial \mathcal{F}}{\partial x_j}[\dot{\bar{\rho}}\dot{\tilde{u}}_i\dot{\tilde{u}}_j - \ddot{\bar{\rho}}\ddot{\tilde{u}}_i\ddot{\tilde{u}}_j + \dot{\tau}(u_i, u_j) - \ddot{\tau}(u_i, u_j) + (\dot{\bar{p}} - \ddot{\bar{p}})\delta_{ij} - (\dot{\tilde{\tau}}_{ij} - \ddot{\tilde{\tau}}_{ij})] \\ & - \frac{\partial}{\partial x_j}\left\{\frac{\partial \mathcal{F}}{\partial x_j}(\dot{\mu}\dot{\tilde{u}}_i - \ddot{\mu}\ddot{\tilde{u}}_i) + \frac{\partial \mathcal{F}}{\partial x_i}(\dot{\mu}\dot{\tilde{u}}_j - \ddot{\mu}\ddot{\tilde{u}}_j) - \frac{2}{3}\frac{\partial \mathcal{F}}{\partial x_k}(\dot{\mu}\dot{\tilde{u}}_k - \ddot{\mu}\ddot{\tilde{u}}_k)\delta_{ij}\right\} + \frac{\partial \mathcal{F}}{\partial t}[\dot{\bar{\rho}}\dot{\tilde{u}}_i - \ddot{\bar{\rho}}\ddot{\tilde{u}}_i]\end{aligned} \tag{2.42}$$

$$\begin{aligned}\sigma_{\rho E} = {} & \frac{\partial \mathcal{F}}{\partial x_j}\left\{\dot{\bar{\rho}}\dot{\tilde{u}}_j\dot{\widetilde{E}} - \ddot{\bar{\rho}}\ddot{\tilde{u}}_j\ddot{\widetilde{E}} + \dot{\tau}(E, u_j) - \ddot{\tau}(E, u_j) + \dot{\tilde{u}}_j\dot{\bar{p}} - \ddot{\tilde{u}}_j\ddot{\bar{p}} + \dot{\chi}(u_j, p) - \ddot{\chi}(u_j, p)\right. \\ & \left. - \left(\dot{\kappa}\frac{\partial \dot{\widetilde{T}}}{\partial x_j} - \ddot{\kappa}\frac{\partial \ddot{\widetilde{T}}}{\partial x_j} + \dot{\chi}\left(\frac{\partial T}{\partial x_j}, \kappa\right) - \ddot{\chi}\left(\frac{\partial T}{\partial x_j}, \kappa\right)\right) - \left(\dot{\tilde{\tau}}_{ij}\dot{\tilde{u}}_i - \ddot{\tilde{\tau}}_{ij}\ddot{\tilde{u}}_i + \dot{\zeta}(\tau_{ij}, u_i) - \ddot{\zeta}(\tau_{ij}, u_i)\right)\right\} + \frac{\partial \mathcal{F}}{\partial t}[\dot{\bar{\rho}}\dot{\widetilde{E}} - \ddot{\bar{\rho}}\ddot{\widetilde{E}}]\end{aligned} \tag{2.43}$$

and

$$\sigma_{\tilde{\tau}(a,b)} = \bar{\rho}\left[\mathcal{F}\left(1 - \mathcal{F}\frac{\dot{\bar{\rho}}}{\bar{\rho}}\right)\frac{\dot{\bar{\rho}}}{\bar{\rho}}\dot{\tilde{a}}\dot{\tilde{b}} - \mathcal{F}(1-\mathcal{F})\frac{\dot{\bar{\rho}}\ddot{\bar{\rho}}}{\bar{\rho}^2}\dot{\tilde{a}}\ddot{\tilde{b}}\right] + \bar{\rho}\left[(1-\mathcal{F})\left(1 - (1-\mathcal{F})\frac{\ddot{\bar{\rho}}}{\bar{\rho}}\right)\frac{\ddot{\bar{\rho}}}{\bar{\rho}}\ddot{\tilde{a}}\ddot{\tilde{b}} - \mathcal{F}(1-\mathcal{F})\frac{\dot{\bar{\rho}}\ddot{\bar{\rho}}}{\bar{\rho}^2}\ddot{\tilde{a}}\dot{\tilde{b}}\right] \tag{2.44}$$

$$\sigma_{\tilde{\chi}(a,b)} = \left[\mathcal{F}\left(1 - \mathcal{F}\frac{\dot{\bar{\rho}}}{\bar{\rho}}\right)\dot{\tilde{a}}\dot{\tilde{b}} - \mathcal{F}(1-\mathcal{F})\frac{\dot{\bar{\rho}}}{\bar{\rho}}\dot{\tilde{a}}\ddot{\tilde{b}}\right] + \left[(1-\mathcal{F})\left(1 - (1-\mathcal{F})\frac{\ddot{\bar{\rho}}}{\bar{\rho}}\right)\ddot{\tilde{a}}\ddot{\tilde{b}} - \mathcal{F}(1-\mathcal{F})\frac{\ddot{\bar{\rho}}}{\bar{\rho}}\ddot{\tilde{a}}\dot{\tilde{b}}\right] \tag{2.45}$$

$$\sigma_{\tilde{\zeta}(a,b)} = \left[\mathcal{F}\left(1 - \mathcal{F}\frac{\dot{\bar{\rho}}^2}{\bar{\rho}^2}\right)\dot{\tilde{a}}\dot{\tilde{b}} - \mathcal{F}(1-\mathcal{F})\frac{\dot{\bar{\rho}}\ddot{\bar{\rho}}}{\bar{\rho}^2}\dot{\tilde{a}}\ddot{\tilde{b}}\right] + \left[(1-\mathcal{F})\left(1 - (1-\mathcal{F})\frac{\ddot{\bar{\rho}}^2}{\bar{\rho}^2}\right)\ddot{\tilde{a}}\ddot{\tilde{b}} - \mathcal{F}(1-\mathcal{F})\frac{\dot{\bar{\rho}}\ddot{\bar{\rho}}}{\bar{\rho}^2}\ddot{\tilde{a}}\dot{\tilde{b}}\right] \tag{2.46}$$

Eqs. (2.41)–(2.43) represent turbulent terms that contribute to the governing equations during the RANS to LES transition (RTLT) zone. They occur due to the incommutability between hybrid operator and differentiation. Similarly, the hybrid terms (Eqs. (2.44)–(2.46)) are also only relevant in the RTLT zone and originate due to the nonlinearity of the hybrid central-moments, and consist of products between RANS and LES variables. In the following, Eqs. (2.41)–(2.46) will be referred to as "hybrid contributions" or "hybrid terms" indistinctly. Note that these terms become infinite if the blending function implemented in the hybrid operator is discontinuous. Therefore, a well defined hybrid formulation requires at least a $C^2(x_i)$ and $C^1(t)$ "$\mathcal{F}$" function.

The hybrid contributions provide the mechanism that keeps the balance between modeled and resolved scales in the RTLT zone, where neither RANS nor LES completely models or resolves the turbulence of the flow. In order to demonstrate this point, let us further analyze the hybrid contributions. To simplify the analysis, Eqs. (2.22) and (2.23) are substituted in Eqs. (2.41)–(2.43), and additionally it is assumed that the turbulence is only weakly affected by compressibility effects, which is a valid assumption provided that the fluctuating Mach number is $Ma' < 0.3$ [45]. Therefore, all density ratios appearing in Eqs. (2.44)–(2.46) can be assumed as unity for this discussion. It is also assumed that the implemented blending

function $\mathcal{F}$ is continuous and function of space only, with bounded first- and second-order derivatives. Under these conditions Eqs. (2.41)–(2.46) reduce to

$$\sigma_\rho = \frac{\partial \mathcal{F}}{\partial x_j}[\dot{\bar{\rho}}\dot{\bar{u}}_j - \ddot{\bar{\rho}}\ddot{\bar{u}}_j], \tag{2.47}$$

$$\sigma_{\rho u_i} = \frac{\partial \mathcal{F}}{\partial x_j}[\overline{\rho u_i}\dot{\overline{u_j}} - \overline{\rho u_i}\ddot{\overline{u_j}} + (\dot{\bar{p}} - \ddot{\bar{p}})\delta_{ij} - (\dot{\bar{\tau}}_{ij} - \ddot{\bar{\tau}}_{ij})] - \frac{\partial}{\partial x_j}\left\{\frac{\partial \mathcal{F}}{\partial x_j}(\dot{\bar{\mu}}\dot{\bar{u}}_i - \ddot{\bar{\mu}}\ddot{\bar{u}}_i) + \frac{\partial \mathcal{F}}{\partial x_i}\left(\dot{\bar{\mu}}\dot{\bar{u}}_j - \ddot{\bar{\mu}}\ddot{\bar{u}}_j\right) - \frac{2}{3}\frac{\partial \mathcal{F}}{\partial x_k}(\dot{\bar{\mu}}\dot{\bar{u}}_k - \ddot{\bar{\mu}}\ddot{\bar{u}}_k)\delta_{ij}\right\}, \tag{2.48}$$

$$\sigma_{\rho E} = \frac{\partial \mathcal{F}}{\partial x_j}\left\{\overline{\rho u_j E}^{\cdot} - \overline{\rho u_j E}^{\cdot\cdot} + \overline{u_j p}^{\cdot} - \overline{u_j p}^{\cdot\cdot} - \left(\overline{\kappa\frac{\partial T}{\partial x_j}}^{\cdot} - \overline{\kappa\frac{\partial T}{\partial x_j}}^{\cdot\cdot}\right) - (\widetilde{\tau_{ij}u_i}^{\cdot} - \widetilde{\tau_{ij}u_i}^{\cdot\cdot})\right\}, \tag{2.49}$$

$$\sigma_{\tilde{\tau}(a,b)} = \frac{\mathcal{F}(1-\mathcal{F})}{\bar{\rho}}(\overline{\rho a}^{\cdot} - \overline{\rho a}^{\cdot\cdot})(\overline{\rho b}^{\cdot} - \overline{\rho b}^{\cdot\cdot}), \tag{2.50}$$

$$\sigma_{\tilde{\chi}(a,b)} = \frac{\mathcal{F}(1-\mathcal{F})}{\bar{\rho}}(\overline{\rho a}^{\cdot} - \overline{\rho a}^{\cdot\cdot})(\dot{\bar{b}} - \ddot{\bar{b}}), \tag{2.51}$$

$$\sigma_{\tilde{\zeta}(a,b)} = \frac{\mathcal{F}(1-\mathcal{F})}{\bar{\rho}^2}(\overline{\rho a}^{\cdot} - \overline{\rho a}^{\cdot\cdot})(\overline{\rho b}^{\cdot} - \overline{\rho b}^{\cdot\cdot}). \tag{2.52}$$

Eqs. (2.47)–(2.52) indicate that the hybrid contributions are directly proportional to difference between RANS and LES variables. In order to extract additional information, the RANS and the LES differences can be approximated with the instantaneous turbulent fluctuation $\phi^{\dot{r}} = \phi - \dot{\bar{\phi}} = \mathcal{C}(\ddot{\bar{\phi}} - \dot{\bar{\phi}})$, since $\ddot{\bar{\phi}} \to \phi$ for $\Delta \to 0$ and $\overline{\phi^{\dot{r}}}^{\cdot} = \mathcal{C}(\dot{\bar{\phi}} - \dot{\bar{\phi}}) = 0$. Here, ϕ is the instantaneous variable and $\mathcal{C}$ is an order one coefficient. Therefore, by substituting $\phi^{\dot{r}} = \mathcal{C}(\ddot{\bar{\phi}} - \dot{\bar{\phi}})$ in Eqs. (2.47)–(2.52) and assuming $\mathcal{C} = 1$ the hybrid contributions can be expressed as

$$\sigma_\rho = -\frac{\partial \mathcal{F}}{\partial x_j}(\rho u_j)^{\dot{r}}, \tag{2.53}$$

$$\sigma_{\rho u_i} = -\frac{\partial \mathcal{F}}{\partial x_j}[(\rho u_i u_j)^{\dot{r}} + p^{\dot{r}}\delta_{ij} - \tau_{ij}^{\dot{r}}] + \frac{\partial}{\partial x_j}\left\{\frac{\partial \mathcal{F}}{\partial x_j}(\mu u_i)^{\dot{r}} + \frac{\partial \mathcal{F}}{\partial x_i}(\mu u_j)^{\dot{r}} - \frac{2}{3}\frac{\partial \mathcal{F}}{\partial x_k}(\mu u_k)^{\dot{r}}\delta_{ij}\right\}, \tag{2.54}$$

$$\sigma_{\rho E} = -\frac{\partial \mathcal{F}}{\partial x_j}\left\{(\rho u_j E)^{\dot{r}} + (u_j p)^{\dot{r}} - \left(\kappa\frac{\partial T}{\partial x_j}\right)^{\dot{r}} - (\tau_{ij}u_i)^{\dot{r}}\right\}, \tag{2.55}$$

$$\sigma_{\tilde{\tau}(a,b)} = \frac{\mathcal{F}(1-\mathcal{F})}{\bar{\rho}}(\rho a)^{\dot{r}}(\rho b)^{\dot{r}}, \tag{2.56}$$

$$\sigma_{\tilde{\chi}(a,b)} = \frac{\mathcal{F}(1-\mathcal{F})}{\bar{\rho}}(\rho a)^{\dot{r}}(b)^{\dot{r}}, \tag{2.57}$$

$$\sigma_{\tilde{\zeta}(a,b)} = \frac{\mathcal{F}(1-\mathcal{F})}{\bar{\rho}^2}(\rho a)^{\dot{r}}(\rho b)^{\dot{r}}. \tag{2.58}$$

Eqs. (2.53)–(2.58) demonstrate that the hybrid contributions represent physical turbulent scales that are not directly accounted by either RANS or LES. Therefore, if Eqs. (2.41)–(2.46) cannot be reconstructed from the hybrid field they have to be either modeled or prescribed. Here we want to stress that Eqs. (2.53)–(2.58) are just an approximation of the hybrid terms and serve the only purpose of illustrate the physical meaning of the hybrid terms. Therefore, Eqs. (2.53)–(2.58) should not be used to compute or model the hybrid terms, here Eqs. (2.53)–(2.58) have to be used instead. It will be shown that the hybrid contribution plays an important role keeping in equilibrium the transition from RANS to LES, and in compensating the turbulence that RANS does not model and that LES does not yet resolve.

2.3. Time dependent hybrid RANS/LES formulation

Although it will not be pursued any further numerically in this paper, it is worth mentioning the case when the hybridization is conducted over time, i.e., $\mathcal{F} = f(t)$, which is relevant for LES simulations that are conducted from an initial steady RANS field:

$$\frac{\partial\bar{\rho}}{\partial t}+\frac{\partial}{\partial x_j}(\bar{\rho}\tilde{u}_j)=\frac{\partial\mathcal{F}}{\partial t}[\dot{\bar{\rho}}-\ddot{\bar{\rho}}]=-\frac{\partial\mathcal{F}}{\partial t}(\rho)^{\dddot{r}}, \tag{2.59}$$

$$\frac{\partial\bar{\rho}\tilde{u}_i}{\partial t}+\frac{\partial}{\partial x_j}(\bar{\rho}\tilde{u}_i\tilde{u}_j+\bar{p}\delta_{ij}-\tilde{\tau}_{ij}+\bar{\tau}(u_i,u_j))=\frac{\partial\mathcal{F}}{\partial t}[\dot{\bar{\rho}}\dot{\tilde{u}}_i-\ddot{\bar{\rho}}\ddot{\tilde{u}}_i]=-\frac{\partial\mathcal{F}}{\partial t}(\rho u_i)^{\dddot{r}}, \tag{2.60}$$

$$\frac{\partial\bar{\rho}\widetilde{E}}{\partial t}+\frac{\partial}{\partial x_j}\left(\bar{\rho}\widetilde{E}\tilde{u}_j+\bar{p}\tilde{u}_j-\bar{\kappa}\frac{\partial\widetilde{T}}{\partial x_j}-\tilde{\tau}_{ij}\tilde{u}_i+\bar{\tau}(E,u_j)+\bar{\chi}(u_j,p)-\bar{\chi}\left(\frac{\partial T}{\partial x_j},\kappa\right)-\bar{\zeta}(\tau_{ij},u_i)\right)=\frac{\partial\mathcal{F}}{\partial t}[\dot{\bar{\rho}}\dot{\widetilde{E}}-\ddot{\bar{\rho}}\ddot{\widetilde{E}}]=-\frac{\partial\mathcal{F}}{\partial t}(\rho E)^{\dddot{r}}. \tag{2.61}$$

Eqs. (2.59)–(2.61) indicate that the transition from a steady RANS to an unsteady LES simulation is promoted by unsteady sources that help to trigger instabilities in the flow that will develop into resolved turbulence. Here, we only speculate that the inclusion of these terms would help to reduce the time it takes for a steady field (used for initialization or used for forced studies) to develop realistic unsteady turbulence.

Note that for time dependent blending functions equation (2.20) will not be valid if the RANS operator represents a time-averaged operator, since in this case the blending function will not commute with the time-averaging operator $\overline{\mathcal{F}\phi}\neq\mathcal{F}\dot{\bar{\phi}}$. Nevertheless, even in this case Eqs. (2.59)–(2.61) are still valid.

2.4. Turbulence modeling

In order to solve the governing equations, the generic hybrid central-moments have to be defined using RANS and LES equations. For RANS, the closure model implemented at present uses a standard eddy viscosity and a gradient diffusion assumption:

$$\dot{\tilde{\tau}}(u_k,u_k)=2\bar{\rho}k \tag{2.62}$$

$$\dot{\tilde{\tau}}(u_i,u_j)=-2\bar{\rho}v_t\left(\widetilde{S}_{ij}-\frac{1}{3}\widetilde{S}_{kk}\delta_{ij}\right)+\frac{2}{3}\bar{\rho}k\delta_{ij} \tag{2.63}$$

$$\dot{\bar{\chi}}\left(\frac{\partial T}{\partial x_j},\kappa\right)+\dot{\bar{\zeta}}(\tau_{ij},u_i)-\dot{\tilde{\tau}}(E,u_j)-\dot{\bar{\chi}}(u_j,p)=\frac{\bar{\rho}C_pv_t}{\mathrm{Pr}_T}\frac{\partial\widetilde{T}}{\partial x_j} \tag{2.64}$$

$$+\bar{\rho}(\bar{\nu}+v_t\sigma^*)\frac{\partial k}{\partial x_j}-\dot{\tilde{\tau}}(u_i,u_j)\tilde{u}_i. \tag{2.65}$$

Here, k is the turbulent kinetic energy (TKE), ν is the kinematic viscosity, v_t is the turbulent eddy viscosity, C_p is the heat capacity at constant pressure, and σ^* and Pr_T are constants set to 1/2 and 1, respectively [46]. Similarly, the same assumptions are used to construct the LES closures defined as

$$\ddot{\tilde{\tau}}(u_k,u_k)=2\bar{\rho}k^{ksgs} \tag{2.66}$$

$$\ddot{\tilde{\tau}}(u_i,u_j)=-2\bar{\rho}v_{sgs}(\widetilde{S}_{ij}-\frac{1}{3}\widetilde{S}_{kk}\delta_{ij})+\frac{2}{3}\bar{\rho}k^{sgs}\delta_{ij} \tag{2.67}$$

$$\ddot{\bar{\chi}}\left(\frac{\partial T}{\partial x_j},\kappa\right)+\ddot{\bar{\zeta}}(\tau_{ij},u_i)-\ddot{\tilde{\tau}}(E,u_j)-\ddot{\bar{\chi}}(u_j,p)=\frac{\bar{\rho}C_pv_{sgs}}{\mathrm{Pr}_t}\frac{\partial\widetilde{T}}{\partial x_j} \tag{2.68}$$

$$+\bar{\rho}\frac{v_{sgs}}{Pr_t}\frac{\partial\widetilde{H}}{\partial x_j}-\ddot{\tilde{\tau}}(u_i,u_j)\tilde{u}_i. \tag{2.69}$$

Here, k^{sgs} is the subgrid kinetic energy, v_{sgs} is the subgrid eddy viscosity, $\widetilde{H}=\widetilde{E}+\bar{p}/\bar{\rho}$ is the total enthalpy, and Pr_t is a coefficient assumed unity [47]. Finally, model equations for v_t, k, v_{sgs}, and k^{sgs} have to be defined to close the system of equations.

2.4.1. Hybrid RANS/LES turbulence model

In this work, RANS and LES turbulence models are coupled in the hybrid formulation by blending equivalent RANS and LES models. Here, we select the two-equation RANS-SST model [48] and the one-equation localized dynamic k^{sgs} (LDKM) LES model [47] to compute v_t, k, v_{sgs}, and k^{sgs} since both methods have transport equations for the kinetic energy of the turbulence (k for RANS and k^{sgs} for LES), which are used to design the hybrid model equation. The RANS-SST model is selected due to its well-documented success predicting complex flows.

An equation for the hybrid turbulent kinetic energy ($\mathcal{K}=\mathcal{F}k+(1-\mathcal{F})k^{sgs}$), can be derived formally by merging RANS and LES transport equations following the same procedure used to derive the hybrid N–S equations. However, this approach would yield an equation with extra terms that cannot be readily computed, and unlike the hybrid N–S equations, it is not possible to demonstrate any physical significance for all the additional terms derived in the hybrid *model* equation. The formal combination of two model equations does not guarantee that the physics of the flow is modeled any better. Here, we propose a model equation that identically recovers the RANS k and LES k^{sgs} equations in such a way that its structure resembles Eqs. (2.35)–(2.37) without the hybrid contributions. This model equation is

$$\frac{\partial\bar{\rho}\mathcal{K}}{\partial t}+\frac{\partial}{\partial x_j}(\bar{\rho}\tilde{u}_j\mathcal{K}-KT_j)=KS, \tag{2.70}$$

where

$$KT_j = \mathcal{F}\left(\bar{\rho}(\bar{\nu}+\sigma_k \nu_t)\frac{\partial \mathcal{K}}{\partial x_j}\right) + (1-\mathcal{F})\left(\bar{\rho}\left(\frac{\bar{\nu}}{Pr}+\nu_{sgs}\right)\frac{\partial \mathcal{K}}{\partial x_j}\right), \tag{2.71a}$$

$$KS = \mathcal{F}\left(-\dot{\tilde{\tau}}(u_i,u_j)\frac{\partial \tilde{u}_i}{\partial x_j} - \beta^*\bar{\rho}\mathcal{K}\omega\right) + (1-\mathcal{F})\left(-\ddot{\tilde{\tau}}(u_i,u_j)\frac{\partial \tilde{u}_i}{\partial x_j} - C_\varepsilon\bar{\rho}\frac{\mathcal{K}^{3/2}}{\Delta}\right). \tag{2.71b}$$

Eq. (2.70) is the model equation for the hybrid turbulent kinetic energy ($\mathcal{K}$). The model equation is constructed by directly blending the source and the transport terms of the RANS-SST "k" and the LES "k^{sgs}" equations. An additional modification is required in Eqs. (2.63) and (2.67) to eliminate their explicit dependence on k and k^{sgs}. Both turbulence variables are substituted by $\mathcal{K}$ so that

$$\dot{\tilde{\tau}}(u_i,u_j) = -2\bar{\rho}\nu_t\left(\widetilde{S}_{ij} - \frac{1}{3}\widetilde{S}_{kk}\delta_{ij}\right) + \frac{2}{3}\bar{\rho}\mathcal{K}\delta_{ij}, \tag{2.72}$$

$$\ddot{\tilde{\tau}}(u_i,u_j) = -2\bar{\rho}\nu_{sgs}\left(\widetilde{S}_{ij} - \frac{1}{3}\widetilde{S}_{kk}\delta_{ij}\right) + \frac{2}{3}\bar{\rho}\mathcal{K}\delta_{ij}. \tag{2.73}$$

This additional modification does not alter the original RANS-SST and LES-LDKM equations, which are identically recovered when $\mathcal{F}=1$ and $\mathcal{F}=0$, respectively. The RANS-SST model requires an additional equation for the specific energy dissipation rate "ω" defined by

$$\frac{\partial}{\partial t}(\bar{\rho}\omega) + \frac{\partial}{\partial x_j}(\bar{\rho}\tilde{u}_j\omega) = -\frac{\gamma}{\nu_t}\dot{\tilde{\tau}}(u_i,u_j)\frac{\partial \tilde{u}_i}{\partial x_j} - \beta\bar{\rho}\omega^2 + \frac{\partial}{\partial x_j}\left[\bar{\rho}(\bar{\nu}+\sigma_\omega\nu_t)\frac{\partial \omega}{\partial x_j}\right] + 2(1-F_1)\bar{\rho}\sigma_{\omega 2}\frac{1}{\omega}\frac{\partial \mathcal{K}}{\partial x_j}\frac{\partial \omega}{\partial x_j}, \tag{2.74}$$

$$F_1 = \tanh(\chi^4), \quad \chi = \min\left(\max\left(\frac{\sqrt{\mathcal{K}}}{0.09\omega y};\frac{500\bar{\nu}}{y^2\omega}\right);\frac{4\bar{\rho}\sigma_{\omega 2}\mathcal{K}}{CDy^2}\right), \tag{2.75a}$$

$$CD = \max\left(2\bar{\rho}\sigma_{\omega 2}\frac{1}{\omega}\frac{\partial \mathcal{K}}{\partial x_j}\frac{\partial \omega}{\partial x_j};10^{-20}\right). \tag{2.75b}$$

Here, Ω, F_1, and y are the vorticity magnitude, a blending function, and the wall-normal distance, respectively. Here, we stress that the equation for ω is not explicitly hybridized since there is no equivalent equation in the LES model implemented here. The constants for the RANS-SST model, here represented as ψ, are computed from two set of constants ψ_1 and ψ_2 as $\psi = F_1\psi_1 + (1-F_1)\psi_2$. Here, the values of these two sets are: $\psi_1\{\sigma_{k1}=0.85,\ \sigma_{\omega 1}=0.5,\ \beta_1=0.075,\ a_1=0.31,\ \beta^*=0.09,\ \kappa=0.41,\ \gamma_1=\beta_1/\beta^*-\sigma_{\omega 1}\kappa^2/\sqrt{\beta^*}\}$ and $\psi_2\{\sigma_{k2}=1.0,\ \sigma_{\omega 2}=0.856,\ \beta_2=0.0828,\ \beta^*=0.09,\ \kappa=0.41,\ \gamma_2=\beta_2/\beta^*-\sigma_{\omega 2}\kappa^2/\sqrt{\beta^*}\}$ [48]. Finally, the RANS and the LES eddy viscosities are defined by

$$\nu_t = \frac{a_1\mathcal{K}}{\max(a_1\omega;\Omega F_2)} \tag{2.76}$$

and

$$\nu_{sgs} = C_\nu \Delta\sqrt{\mathcal{K}}, \tag{2.77}$$

where

$$F_2 = \tanh(\eta^2), \quad \eta = \max\left(2\frac{\sqrt{\mathcal{K}}}{0.09\omega y};\frac{500\bar{\nu}}{y^2\omega}\right). \tag{2.78}$$

Here, C_ν and C_ϵ are LES coefficients that are obtained dynamically as a part of the solution using a scale similarity approach [47].

3. Validation of the hybrid RANS/LES formulation

In order to evaluate the importance of the hybrid terms, Eqs. (2.41)–(2.45), LES and hybrid RANS/LES simulations are conducted for the turbulent attached flow over a flat-plate at $Re_\theta = 1430$, based on the boundary layer momentum thickness (θ) and free stream velocity (U_∞). These conditions correspond to the experimental data of DeGraaff and Eaton [49]. For this case the approximate Reynolds number based on the friction velocity is around $Re_\tau \sim 500$ which is about the same used in a previous hybrid RANS/LES study conducted in channel flow [22].

The main objective here is to demonstrate the importance of the hybrid terms. Therefore, when needed, these terms are a priori computed from the LES simulation. Here it is important to stress, that even if in theory the LES field could be computed with Eq. (2.21) and from it the hybrid terms, it is very likely that Eq. (2.21) could become ill-conditioned, and thus, numerically intractable [39]. Even if Eq. (2.21) converge in all the domain, the LES field could not be correctly recovered since the grid resolution expected to be used in engineering applications would be too coarse to allow the LES reconstruction. Therefore, for practical applications the only way to include Eqs. (2.41)–(2.46) is through modeling. However, in this work we are

interested only to identify and highlight the fundamental importance of the hybrid terms in this hybrid RANS/LES formulation. Therefore, explicit models for Eqs. (2.41)–(2.46) are not discussed but they are currently being pursued.

3.1. Numerical approach

Accurate LES simulations require high order discretization in both time and space. Therefore, the governing equations and the turbulence models are solved with a parallel code consisting of a fully coupled explicit compressible finite volume formulation, where time integration is conducted using a five stage Runge–Kutta scheme [50] and space discretization uses a fourth-order scheme in divergence form [51]. Additionally, to prevent spurious numerical oscillations an explicit tenth-order low-pass filter is applied periodically to the flow variables based on an approach demonstrated earlier [52].

Boundary conditions are applied explicitly for the flow and the turbulence variables. At the wall, no-slip and adiabatic conditions are imposed. At the free stream boundary, the variables are computed from the one-dimensional Riemann invariants [53]. In the spanwise direction, periodic boundary conditions are implemented, and at the outflow, a zero gradient condition is enforced. For the LES simulation, realistic turbulence is provided at the inflow boundary by using the rescaling method of Lund et al. [54]. For the hybrid RANS/LES simulations the turbulent inflow is obtained from a LES simulation that is conducted simultaneously. Here, we did not notice significant differences when the rescaling approach of Lund was implemented in the hybrid field.

Based on previous LES [54] and DNS [55] studies, four grids, summarized in Table 1, extending over a domain of $L_x = 10\delta$ (streamwise), $L_y = 3\delta$ (wall-normal), and $L_z = 2\delta$ (spanwise) are evaluated. Here, δ is the boundary layer thickness. For all the grids the grid-points are distributed uniformly in the streamwise and in the spanwise directions, while in the wall-normal direction a hyperbolic tangent stretching is implemented [56]. The benchmark LES simulation is conducted using the fine grid only to capture the near-wall structures [2], while the hybrid RANS/LES simulations are conducted in the four grids.

3.2. Hybrid RANS/LES blending functions

The LES and hybrid RANS/LES simulations are conducted by solving the hybrid governing Eqs (2.35) and (2.40), the generic central-moments Eqs. (2.25)–(2.27), and the turbulent hybrid model Eqs. (2.70)–(2.78) with a hybrid blending function $\mathcal{F}$. For LES, $\mathcal{F} \equiv 0$. However, for the hybrid formulation a general specification of the blending function for different flows remains an open issue. Fortunately, for the turbulent boundary layer, it is possible to implement simple blending functions that depend only on the wall-normal distance (thus, principally 1D). Therefore, the sensibility of the model to the blending function can be evaluated without complicating the problem any further.

Five blending functions, summarized on Table 2, are evaluated. The first and second blending functions are constructed using a smooth function to transit from RANS to LES [35].

$$F(y) = \frac{1}{2}\left[1 - \tanh\left(\frac{C_1(y/d - C_2)}{(1-2C_2)y/d + C_2}\right) \Big/ \tanh(C_1)\right]. \tag{3.1}$$

Here, C_1 and C_2 are constants, selected to be 2 and 0.2, respectively. Also, the distance d represents the location at which the blending function is zero, $F(d) = 0$. The first blending function implements Eq. (3.1) over one-quarter of the wall-normal length $d = L_y/4$, so that the boundary layer buffer-layer is within the RTLT zone (this zone is more precisely defined here as the range where $0.9 < \mathcal{F} < 0.1$),

$$\mathcal{F}1(y) = \begin{cases} F(y) & \text{for } y \leqslant d = L_y/4 \\ 0 & \text{for} y > d \end{cases} \tag{3.2}$$

The second blending function is designed to use Eq. (3.1) throughout the domain $d = L_y$, to set the outer layer within the RTLT zone, so that

$$\mathcal{F}2(y) = F(y), \quad d = L_y. \tag{3.3}$$

The third blending function consists of a linear function with limits $L_1 = L_y/100$ and $L_2 = L_y/3$ which bounds a RANS zone between $0 \leqslant y^+ < 20$, the RTLT region between $20 \leqslant y^+ \leqslant 580$ and the LES zone beyond $y^+ > 580$,

Table 1
Summary of grids implemented.

Grid name	Number of grid points	Grid resolution			
	$n_x \times n_y \times n_z$	Δx^+	Δy^+_{min}	Δy^+_{max}	Δz^+
Fine	$201 \times 91 \times 121$	30	0.5	63	10
Medium	$201 \times 45 \times 121$	30	0.5	147	10
Coarse	$201 \times 45 \times 65$	30	0.5	147	20
Coarsest	$151 \times 25 \times 65$	40	0.5	300	20

Table 2
Summary of hybrid RANS/LES blending functions.

Formulation	Blending function	RTLT zone	Equation
	$\mathcal{F}$	$0.1 < \mathcal{F} < 0.9$	
RANS	1	Does not apply	–
LES	0	Does not apply	–
Hybrid RANS/LES	$\mathcal{F}1$	$8 < y^+ < 40$	(3.2)
Hybrid RANS/LES	$\mathcal{F}2$	$30 < y^+ < 240$	(3.3)
Hybrid RANS/LES	$\mathcal{F}3$	$20 < y^+ < 580$	(3.4)
Hybrid RANS/LES	$\mathcal{F}4$	$50 < y^+ < 1100$	(3.5)
Zonal RANS/LES	$\mathcal{F}^{step}$	Discontinuous	(3.6)

$$\mathcal{F}3(y) = \begin{cases} 1 & \text{for } y \leqslant L_1 \\ 1 - (y - L_1)/(L_2 - L_1) & \text{for } L_1 \leqslant y \leqslant L_2 \\ 0 & \text{for } y > L_2 \end{cases} \tag{3.4}$$

The fourth blending function consist of an exponentially decaying cosine function. This function completes 2.5 cycles throughout the domain inducing five RTLT zones, the objective is to evaluate the effect of nonmonotonic function which induces multiples RTLT regions in the domain,

$$\mathcal{F}4(y) = e^{-y/L_y}[\cos(5\pi y/L_y) + 1]/2. \tag{3.5}$$

Finally, the fifth blending function consists of a step function, which leads to the classic zonal RANS/LES approach [2,22,23,25–29]. Here, the interface between RANS and LES is specified at $y^+ = 45$, in order to model the inner layer with RANS while the outer layer is resolved with LES. This is consistent with past studies [22,26,28,29], the function is defined as

$$\mathcal{F}^{\text{step}}(y^+) = \begin{cases} 1, & \text{if } y^+ < 45, \\ ,0 & \text{if } y^+ \geqslant 45. \end{cases} \tag{3.6}$$

The five blending functions and the law-of-the-wall, are shown in Fig. 1 normalized by wall-units, $U^+ = U/u_\tau$, $y^+ = yu_\tau/\nu$, where $u_\tau = \sqrt{\tau_w/\rho}$ is the friction velocity. This figure illustrates how the different transition functions blend RANS and LES formulations, and more importantly, Fig. 1 shows the location of RTLT zone superimposed in the law-of-the-wall velocity profile. For $\mathcal{F} \equiv \mathcal{F}1$, the RTLT zone is designed to cover most of the inner layer $8 < y^+ < 40$ to allow LES to resolve part of the energy produced in the buffer layer. For $\mathcal{F} \equiv \mathcal{F}2$, the RTLT zone is located in the outer layer $30 < y^+ < 240$ to guarantee that most of the inner layer is modeled with RANS with a well defined RTLT zone. For $\mathcal{F} \equiv \mathcal{F}3$ the RANS region is extended up to $y^+ \sim 20$ to warrant that most of the near-wall turbulence is modeled with RANS, additionally, the RTLT is designed to cover the outer layer $20 \leqslant y^+ \leqslant 580$ to ensure that most of the boundary layer is simulated with the model in the hybrid mode i.e. $0 < \mathcal{F} < 1$. For $\mathcal{F} \equiv \mathcal{F}4$ the RTLT zone extends from $y^+ = 55$ up to the free stream boundary, in addition, this function reach LES ($\mathcal{F} = 0$) at three locations $y^+ \sim 330$, $y^+ \sim 1000$, and $y^+ \sim 1700$. Finally, for $\mathcal{F} \equiv \mathcal{F}^{\text{step}}$, the RANS to LES transition point is located at the end of the inner layer to guarantee that RANS completely model this region, this function does not have a RTLT zone.

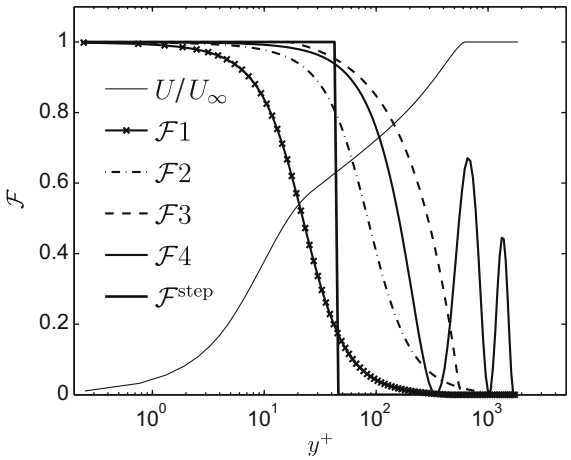

Fig. 1. Law-of-the-wall profile and hybrid RANS/LES blending functions.

3.3. Results and discussion

The initial conditions chosen for $Re_\theta = 1430$ consist of random noise superimposed on the law-of-the-wall profile. This artificial flow field is evolved using periodic boundary conditions in the streamwise direction to promote transition to turbulence. Once realistic turbulence develop, the flow field is rescaled and then used to initialize the LES and hybrid simulations, it is at this point when the rescaling approach of Lund et al. [54] is used to provide turbulent inflow conditions. All the simulations are run initially for a nondimensional period of $t_{\text{trans}} u_\tau^2/\nu_{\text{wall}} \sim 1000$ to eliminate the transient conditions [54]. Here, ν_{wall} is the kinematic viscosity evaluated at the wall. After the flow reach a stationary state, flow statistics are collected for a nondimensional period of $t_{\text{aver}} u_\tau^2/\nu_{\text{wall}} \sim 1800$ [54].

All simulations conducted with the fine grid are summarized in Table 3. The main differences among hybrid RANS/LES simulations are in the blending function implemented, and whether the hybrid contributions are included (hereafter, denoted HRL when the hybrid terms are not considered and HRL-HT when the hybrid terms are included). These terms are computed from the available LES and its time-averaged fields using Eqs. (2.41)–(2.46). For the coarse grids, the hybrid terms are still computed from the LES simulation conducted in the fine grid and then interpolated into the coarse grids.

The mean streamwise velocity profiles (normalized with wall-units) and its wall normal gradient are presented in Fig. 2. Here, the LES prediction is found in excellent agreement with experiments as expected. Interesting to note is that Fig. 2(a) apparently indicates that for the fine grid, the zonal RANS/LES approach (simulation 2 with $\mathcal{F} \equiv \mathcal{F}^{step}$) predicts accurately the mean velocity profile. This high accuracy of the zonal RANS/LES simulation is explained first by the high resolution used in the fine grid, and second by the fact that RANS, which is calibrated to predict correctly this kind of flows, completely model the inner-layer, whereas LES is able to resolve the turbulence located in the outer-layer region. However, if we analyze the velocity normal gradient, Fig. 2(b), it is evident that the zonal RANS/LES approach predicts an unphysical flow field which is indicated by the spike located at the models interface ($y^+ = 45$). Here, the anomalous region is bounded within a small region, in the order of 10 wall-units, neighboring the models interface, set at $y^+ = 45$ for this study. However, as will be shown later, if the grid resolution is reduced the error region will be significantly magnified [8,22,26,28,29]. This is a well-documented anomaly observed in all zonal RANS/LES approaches [8,22], and it is due to the abrupt switch from RANS to LES. This abrupt switch induces a transition from RANS to LES out of equilibrium. Such that the turbulence is neither completely modeled by RANS nor completely resolved by LES [8].

For HRL-HT simulations Fig. 2 demonstrates that the predicted mean velocity profiles are again in excellent agreement with experiments and the LES simulation. Here, only the line function, simulation 9, presents slight deviations compared with the other functions. However, here we recall that $\mathcal{F}3$ sets RANS modeling at the inner layer and extends the RTLT zone throughout the boundary layer completing the transition to LES at the free stream region. Consequently $\mathcal{F}3$ is the most stringent function here implemented since for most of the boundary layer the turbulence model is acting in the hybrid mode $0 < \mathcal{F} < 1$. Nevertheless, it can be concluded from these results, that as long as the hybrid terms are included the predicted velocity profiles are not very sensitive to the blending function implemented, even when none-monotonic functions with multiples RTLT zones are considered. This implies that during RTLT zone, the turbulence that is not modeled by RANS and is not yet resolved by LES is explicitly accounted by Eqs. (2.41)–(2.46). Therefore, the mean transfer of turbulence throughout the boundary layer is correctly reproduced, and the transition from RANS to LES in the mean velocity profile occurs nearly independent of the blending function implemented.

Fig. 2 also demonstrate that by not including the hybrid contributions (simulations 3–6) the predicted velocity profile becomes very sensitive to the blending function implemented. This is explained by the fact that the amount of modeled and resolved turbulence provided by the hybrid model depends primarily on the blending function. Simulation 3 uses a blending function that sets the RTLT in the inner layer. Therefore, the turbulence not accounted by the hybrid contributions is partially resolved by the LES part of the hybrid model, yielding results in close agreement to LES and simulation 7. On the other hand, simulations 4–6 implement blending functions that set the RTLT deeper in the outer layer, precluding the LES

Table 3
Simulation description and predicted friction coefficient for turbulent boundary layer $R_\theta = 1430$, fine grid.

Simulation	Blending function, $\mathcal{F}$	$C_f \times 10^3$	Deviation from LES (%)
Experiments	–	3.96[a]	–
1 LES	0	4.00	–
2 Zonal RANS/LES	$\mathcal{F}^{step}$	3.92	−2.0
3 HRL	$\mathcal{F}1$	3.81	−4.8
4 HRL	$\mathcal{F}2$	3.44	−14.0
5 HRL	$\mathcal{F}3$	3.46	−13.5
6 HRL	$\mathcal{F}4$	3.50	−12.5
7 HRL-HT	$\mathcal{F}1$	3.77	−5.8
8 HRL-HT	$\mathcal{F}2$	3.88	−3.0
9 HRL-HT	$\mathcal{F}3$	3.73	−6.8
10 HRL-HT	$\mathcal{F}4$	3.94	−1.5

[a] Obtained by best fitting the law-of-the-wall to the experimental data.

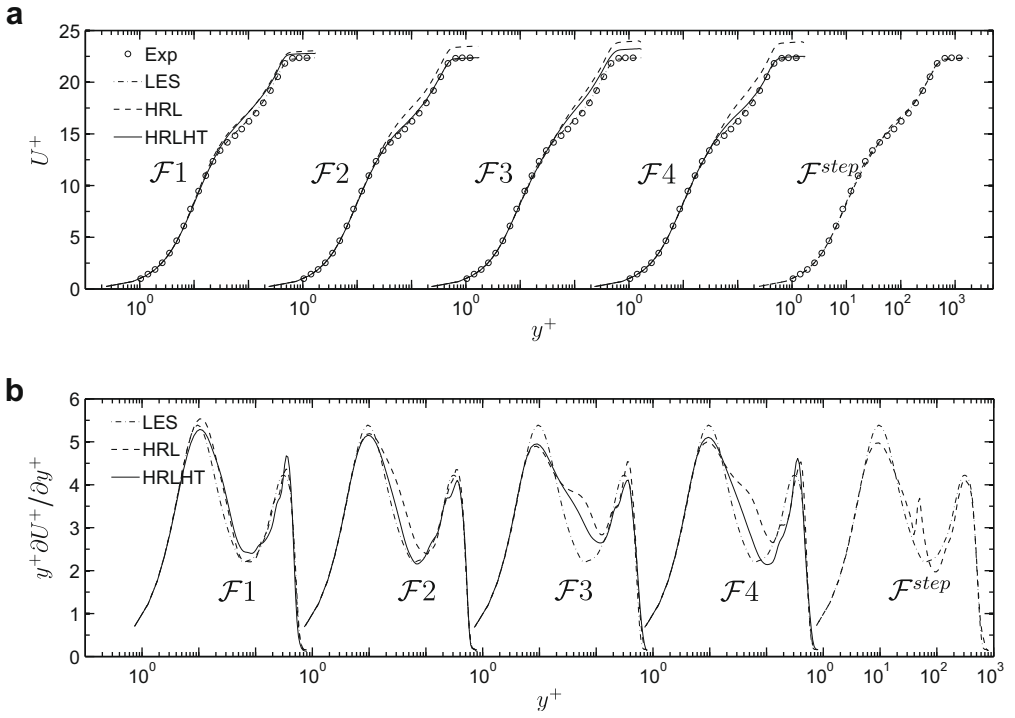

Fig. 2. Wall-normal distribution of mean streamwise-velocity profile and $y^+\partial U^+/\partial y^+$ for LES, HRL, HRL-HT, and Zonal RANS/LES ($\mathcal{F}^{step}$) fine grid simulations: (a) U^+ and (b) $y^+\partial U^+/\partial y^+$.

part of the hybrid model to resolve a significant amount of the turbulence that Eqs. (2.41)–(2.46) represent, resulting in the underprediction of the velocity profiles in Fig. 2(a).

Table 3 shows the friction coefficient (C_f) predicted with the five blending functions using the fine grid. In particular, the friction coefficient computed with LES is found in excellent agreement with the experimental data, previous LES simulations have reported similar accuracy in their calculations [54]. Consequently, we use this LES results as a benchmark reference to analyze the hybrid simulations results.

The zonal approach, simulation 2, predicts a C_f in close agreement with LES. This is an expected result, as mentioned before, since the inner layer is completely modeled by RANS, which is calibrated to reproduce the law-of-the-wall [46,48]. For HRL-HT, simulations 7 to 10, the predicted frictions coefficients are found within -1.5% to -6.8% error respect to LES. The difference among HRL-HT simulations is caused by the different blending functions, which indicates that even when the hybrid terms are included small variations in the predicted C_f can be reproduced with different blending functions. However, when the hybrid contributions are not included significant deviations in the predicted C_f are reproduced among blending functions. Simulation 3 predicts an error with respect to LES (here, the inner-layer of the boundary layer is partially resolved) in close agreement with the error predicted when the hybrid contributions are included (simulation 7). However, if the blending function locates the RTLT away from the inner layer the hybrid model is not able to significantly compensate for the lost turbulence magnifying the deviations in the predicted friction coefficient. For simulation 4 the $\mathcal{F}2$ sets the RTLT zone in $30 < y^+ < 240$ inducing an error, with respect to LES, 4.6 times higher that the error predicted when the hybrid terms are included. For simulation 5 the $\mathcal{F}3$ sets the RTLT zone in $20 < y^+ < 580$, in this case the error is doubled. Here, we point out that this apparent good response of $\mathcal{F}3$ to not including the hybrid terms is misleading, since overall the accuracy of C_f predicted with this function is the lowest for both HRL and HRL-HT simulations. Nevertheless, including the hybrid contributions with this function does have a positive effect improving the accuracy of C_f. For simulation 6 the $\mathcal{F}4$ induces five RTLT regions and yield an error about 8 times higher than when the hybrid terms are included, this drastic drop in accuracy is related with the fact that the multiples RTLT zones make the accuracy of the hybrid formulation more dependent on the hybrid contributions, thus neglecting Eqs. (2.41)–(2.46) has a major effect in the accuracy of C_f. Here we point out that, the behaviour previously described is induced only by the turbulent modeling approach here described, since the grid implemented is fine enough for both LES and RANS simulations. However, a similar trend is observed in the predicted C_f computed with the medium and coarse grids which are not reported here for the sake of brevity.

In order to further elucidate the effect of the blending function and the hybrid contribution in the boundary layer turbulence, the second-order statistics are computed and analyzed. Figs. 3 and 4 presents the resolved Reynolds stresses $\overline{\rho u_i' u_j'}/\dot{\bar{\rho}}$ and the time average of the modeled Reynolds stresses (here after referred just as modeled) $\dot{\bar{\tau}}(u_i, u_j)/\dot{\bar{\rho}}$, respectively, while

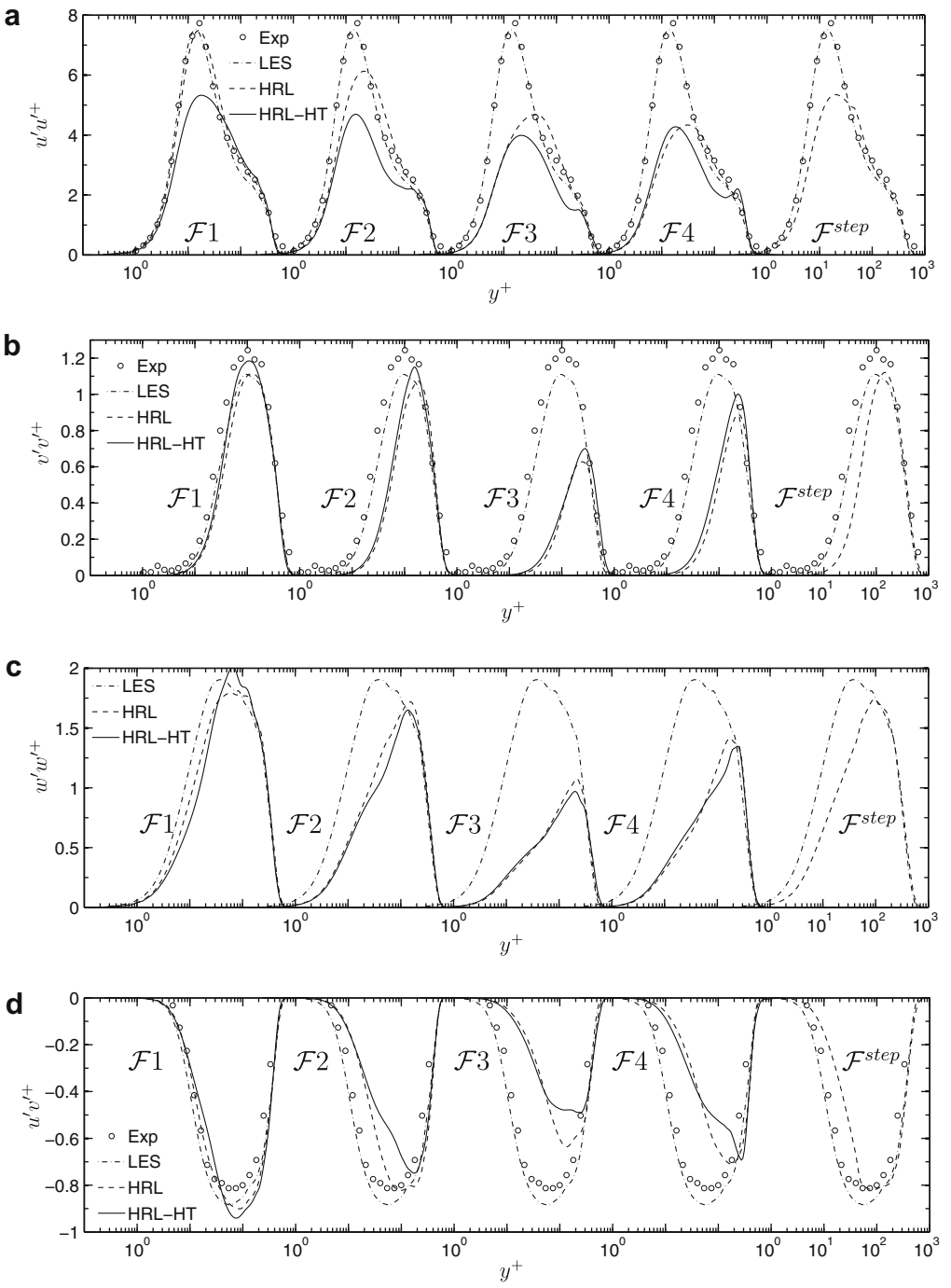

Fig. 3. Wall-normal distribution of resolved Reynolds stresses for LES, HRL, HRL-HT, and Zonal RANS/LES ($\mathcal{F}^{step}$) fine grid simulations: (a) $u'u'^{+}$; (b) $v'v'^{+}$; (c) $w'w'^{+}$; and (d) $u'v'^{+}$.

Fig. 5 presents the total stresses $u_i'u_j'^{tot} = (\overline{\rho u_i' u_j'} + \bar{\bar{\tau}}(u_i, u_j))/\bar{\rho}$ (hereafter we use the notation $u_i'u_j'$ to refer the components of the Reynolds stress tensor indistinctly), for both figures the statistics are computed from the LES and the hybrid RANS/LES formulation on the fine grid. Here, we point out that for the HRL-HT simulations only a fraction, Eq. (2.44), of the hybrid terms Eqs. (2.41)–(2.46) can be included in the modeled stresses. Nevertheless, the rest of the hybrid terms play their part in the governing equations.

As expected, the fine grid allows LES to resolve the near-wall turbulence without any special wall-treatment. Consequently, the LES predictions are found in very-good agreement with the experimental data, as shown in Figs. 3–5, and will

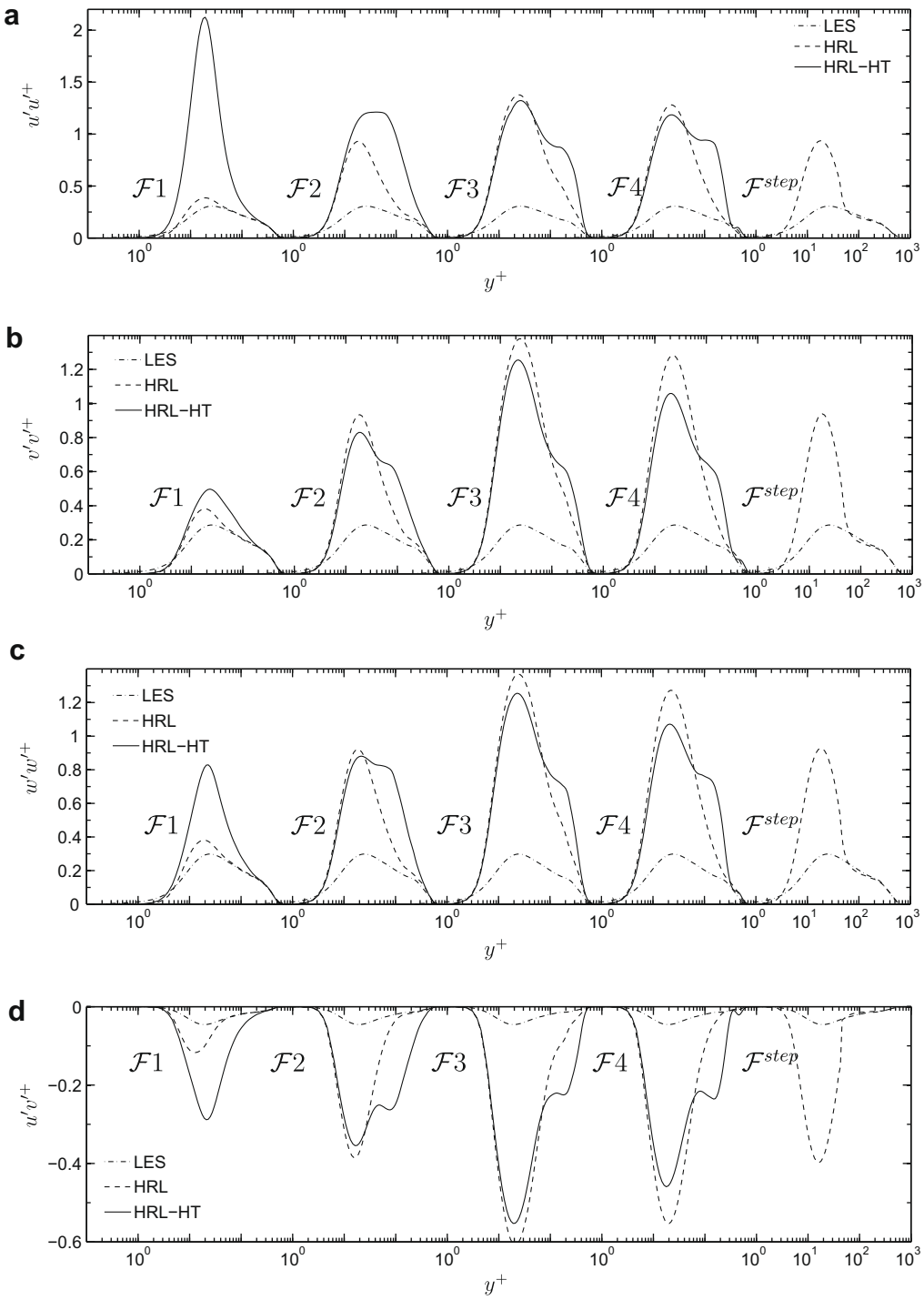

Fig. 4. Wall-normal distribution of modeled Reynolds stresses for LES, HRL, HRL-HT, and Zonal RANS/LES ($\mathcal{F}^{step}$) fine grid simulations: (a) $u'u'^{+}$; (b) $v'v'^{+}$; (c) $w'w'^{+}$; and (d) $u'v'^{+}$.

be used as our benchmark case. For hybrid RANS/LES simulations Figs. 3 and 4 demonstrates the effect that the blending function has on the resolved and modeled Reynolds stresses. Although it is an expected result, Figs. 3 and 4 demonstrates that as the RTLT region gets closer to the wall ($\mathcal{F}4 \rightarrow \mathcal{F}1$) the levels of modeled turbulence drops while the resolved increases, with or without the hybrid terms. This is explained by the fact that LES takes over the hybrid formulation as the RTLT zone completes closer and closer to the near-wall region, replacing modeled by resolved stresses.

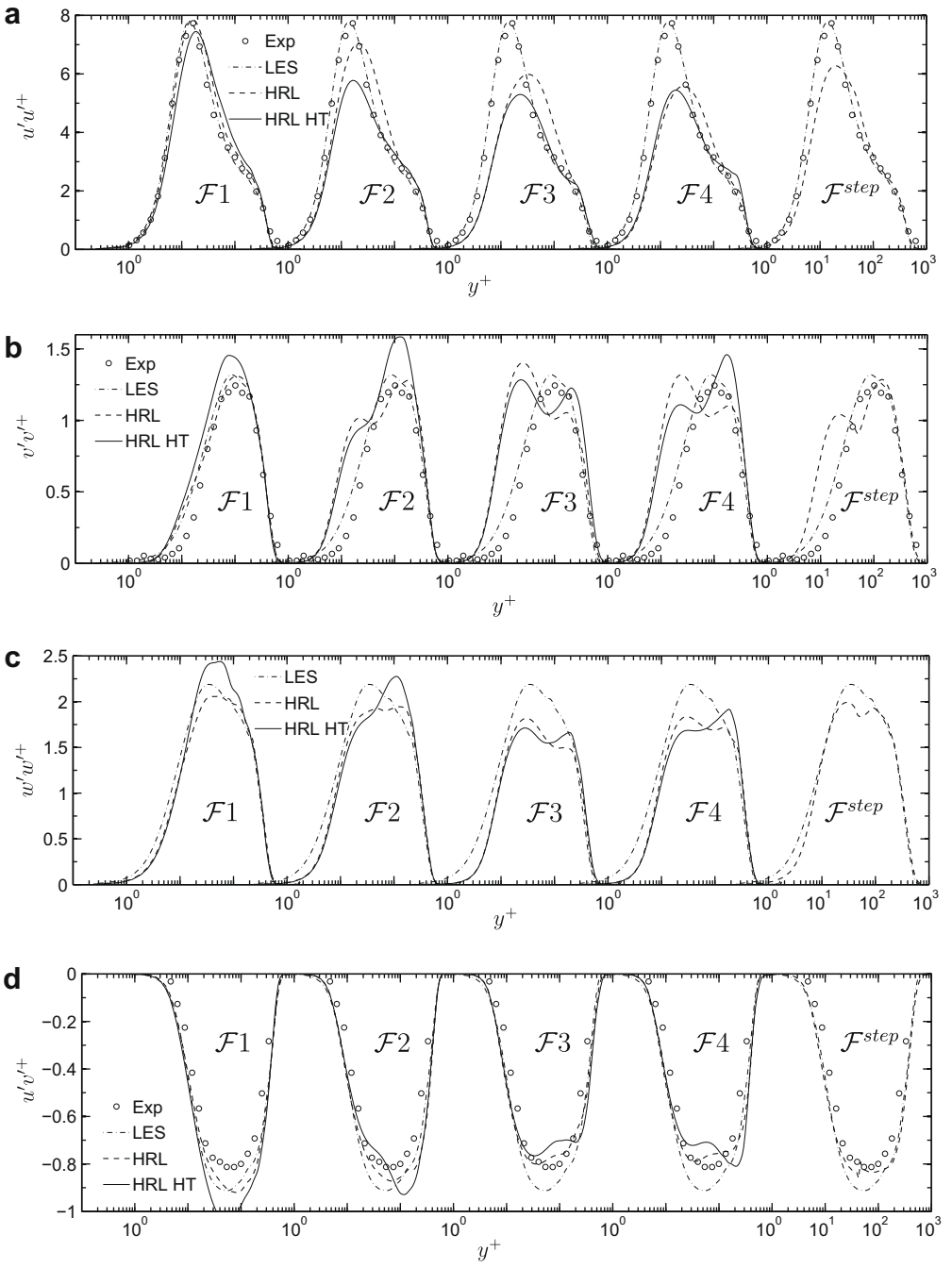

Fig. 5. Wall-normal distribution of total (resolved plus modeled) Reynolds stresses for LES, HRL, HRL-HT, and Zonal RANS/LES ($\mathcal{F}^{step}$) fine grid simulations: (a) $u'u'^{+}$; (b) $v'v'^{+}$; (c) $w'w'^{+}$; and (d) $u'v'^{+}$.

Figs. 3–5 indicate that if discontinuous blending functions are implemented, as in simulation 2, the sharp transition from RANS to LES induces nonphysical discontinuities in the modeled and resolved statistics. Fig. 6 presents the wall-normal derivative of the total principal Reynolds stress $y^{+}\partial u'v'^{+}/\partial y^{+}$ (the other stresses present similar trends). The figure clearly shows, similarly to Fig. 2(b), that only with the step function anomalous profiles, indicated by a spike located precisely at the model interface, are reproduced. Similar discontinuities have been reported in previous hybrid zonal approaches [22,8,36]. The discontinuities in the modeled stresses can be also observed in Fig. 4, which shows the sharp drop of modeled stresses occurring at $y^{+} = 45$ when $\mathcal{F}^{step}$ is used, while with continuous blending functions the modeled stresses smoothly transit from RANS to LES with and without hybrid terms. Similarly, when $\mathcal{F}^{step}$ is used, the resolved stresses, Fig. 3, also

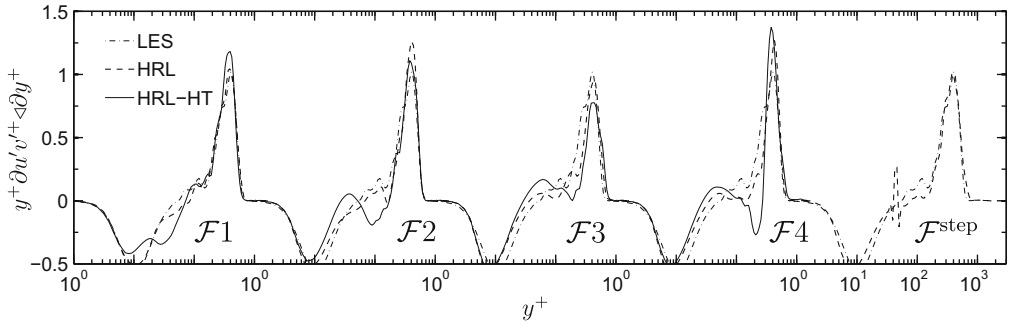

Fig. 6. Wall-normal distribution of $y^+\partial u'v'^+/\partial y^+$ (for the total Reynolds stress, modeled plus resolved) for LES, HRL, HRL-HT, and Zonal RANS/LES ($\mathcal{F}^{step}$) simulations, fine grid results.

present discontinuities. However, they do not go from resolved LES levels to zero at the RANS region as could be expected. In fact, at the RANS region the resolved unsteady structures are not entirely dissipated as indicated by the low, yet not zero, levels of resolved turbulence below $y^+ < 45$. This indicates, that for the zonal RANS/LES approach LES feeds in turbulent unsteady structures, which transform the, otherwise steady, RANS region into a quasi-steady zone. Similarly, nonzero levels of resolved stresses are reproduced within the RANS region with other blending functions, indicating that the existence of a quasi-steady RANS field is not exclusive of zonal RANS/LES approaches.

For HRL and HRL-HT simulations Figs. 3–6 indicate that whether or not the hybrid terms are included, the modeled and resolved statistics do not present any discontinuities in their profiles as long as the blending function is continuous. Figs. 3 and 4 illustrate the distribution of modeled and resolved stresses, which depend on the blending function implemented and whether or not the hybrid contributions are included. However, for the total stresses, shown in Fig. 5, the dependency on blending function and hybrid contribution is not that evident and only quantitative differences can be distinguished.

It is important to mention that the total stresses computed with and without hybrid contributions, with the exception of $u'u'$, present inflection points and a local minimum at the RTLT zone. The inflection point and local minimum are generated because the resolved and modeled stresses do not peak around the same location. Fig. 5 indicates that the peaks's separation distance is found to be in the order of 100 wall units for all blending functions. For the $u'u'$ stress, the modeled and resolved stresses peak around the same location with all blending functions, therefore no local minimum or inflection point is reproduced in this stress. It is important to point out that when the RTLT zone is in the inner-layer, $\mathcal{F}1$, the total stresses do not present any inflection points and local minimum, since the modeled stresses are not that significant when compared with the resolved stresses, for this blending function. Finally, current results indicate that the local minimum and inflection point observed in the total stresses, computed with and without the hybrid contributions, cannot be avoided when blending functions with RTLT in the outer layer are implemented.

Fig. 3 shows that for blending functions with RTLT zone close to the inner-layer, $\mathcal{F}1$, the LES part of the hybrid model is able to resolve a significant amount of the near-wall turbulence yielding resolved stresses in close agreement when the hybrid contributions are included or neglected ($u'u'$ is the only stress that shows slight differences when the hybrid terms are included). In the other hand, Fig. 4 shows that the modeled stresses reach higher values when the hybrid terms are included than when these terms are neglected, slightly increasing the total stresses as seen in Fig. 5. Nonetheless, it can be concluded that for blending functions with RTLT zones located very close to the near-wall region, the effect of the hybrid terms is reduced as indicated in Figs. 2–5 and it is expected that their effect become negligible as $\mathcal{F} \to 0$ everywhere. Contrary, if the blending function locates the RTLT zone in the outer-layer the hybrid contributions become more relevant. Fig. 4 shows that for blending functions $\mathcal{F}2$, $\mathcal{F}3$, and $\mathcal{F}4$ the hybrid contributions indeed increase the modeled stresses in the RTLT zone. This demonstrates that the hybrid terms represent modeled scales that should not be neglected. In fact, if these terms are neglected, the levels of modeled stresses drops and the hybrid model is forced to compensate this deficit by resolving more scales as seen, specially with $u'u'$ and $u'v'$, in Fig. 3. Unfortunately, for RTLT zones deep in the outer-layer, the LES part of the hybrid model is not able to correctly compensate Eqs. (2.41)–(2.46) yielding levels of resolved and modeled stresses that differs from those computed with the hybrid contributions, which eventually leads to the inaccurate predictions in the mean velocity profile and C_f.

Whether, the blending function allows the hybrid model to resolve part of the turbulence contained in the hybrid contributions, these terms cannot be completely resolved by the LES part of the hybrid formulation unless the blending function reduces to $\mathcal{F} \equiv 0$ everywhere, which obviously reduces the hybrid RANS/LES formulation to LES. Therefore, if Eqs. (2.41)–(2.46) are neglected and $\mathcal{F}$ is not always zero some amount of turbulence, that cannot be resolved nor modeled, is lost. How much turbulence is not accounted in the hybrid simulations and how this impacts the accuracy of the calculations strongly depends on the blending function implemented. This is the main reason why the flow statistics predicted with the five blending functions here implemented (simulations 2–6) differ from each others.

Figs. 7–9 show the effect of the hybrid formulation in the instantaneous velocity field. It presents the velocity fluctuations, plotted over the spanwise direction, normalized with the free stream velocity sampled at the buffer layer $y^+ = 11$ and at the

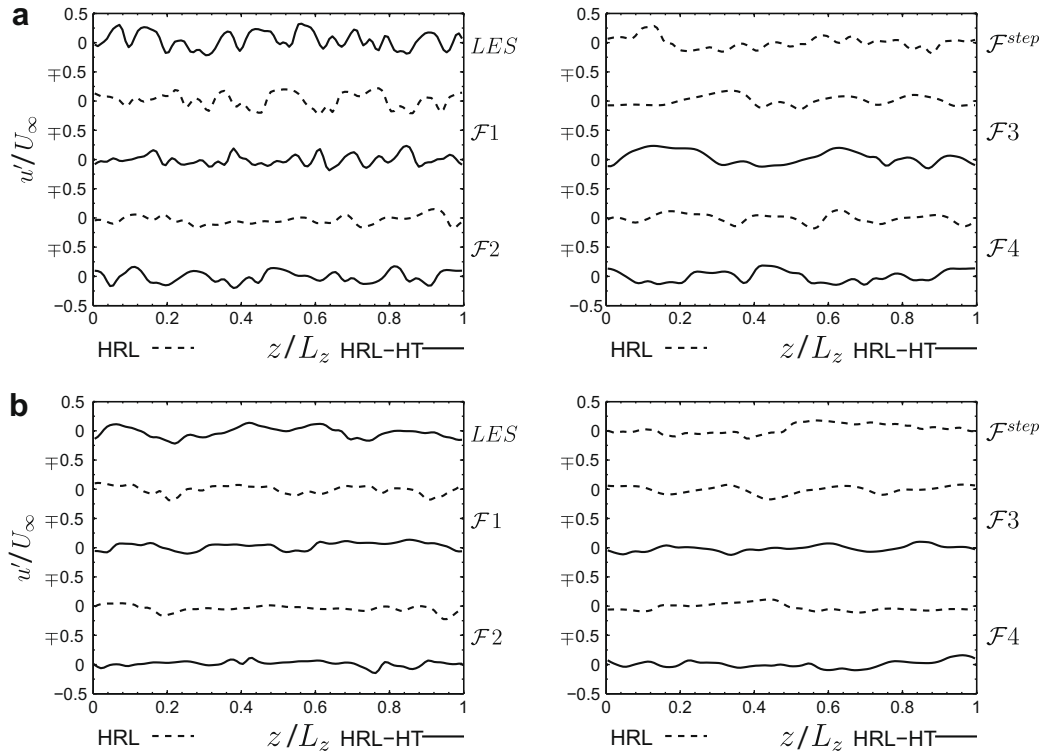

Fig. 7. Spanwise distribution of normalized unsteady streamwise-velocity fluctuations u'/U_∞ for LES, HRL, HRL-HT, and Zonal RANS/LES ($\mathcal{F}^{step}$) fine grid simulations: (a) wall-normal location $y^+ = 11$, RANS-dominated region for all blending functions and (b) wall-normal location $y^+ = 100$, RANS-dominated region for $\mathcal{F}3$ and $\mathcal{F}4$ functions. Here the y-axis is shifted to show all the plots.

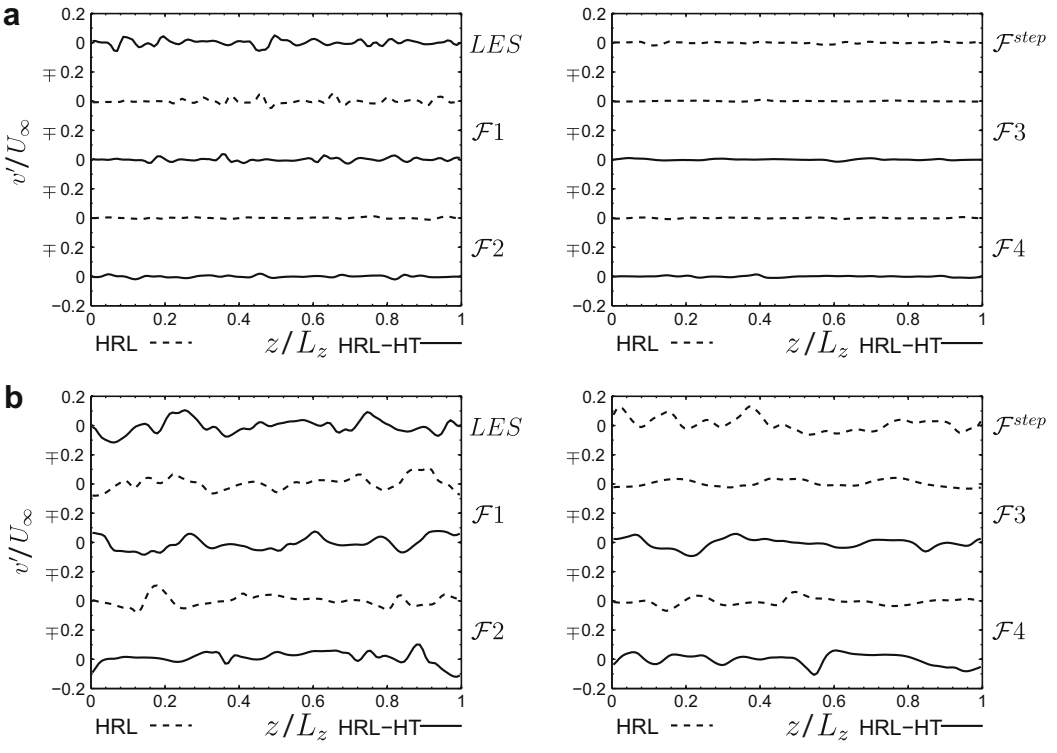

Fig. 8. Spanwise distribution of normalized unsteady wall-normal-velocity fluctuations v'/U_∞ for LES, HRL, HRL-HT, and Zonal RANS/LES ($\mathcal{F}^{step}$) fine grid simulations: (a) wall-normal location $y^+ = 11$, RANS-dominated region for all blending functions and (b) wall-normal location $y^+ = 100$, RANS-dominated region for $\mathcal{F}3$ and $\mathcal{F}4$ functions. Here, the y-axis is shifted to show all the plots.

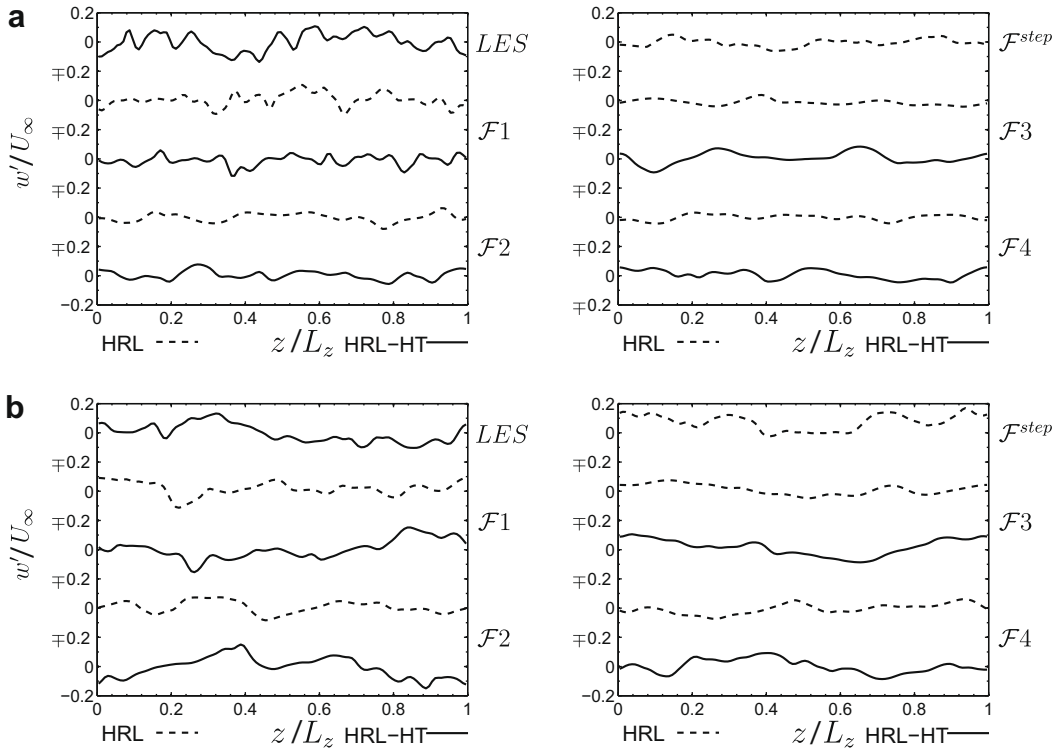

Fig. 9. Spanwise distribution of normalized unsteady spanwise-velocity fluctuations w/U_∞ for LES, HRL, HRL-HT, and Zonal RANS/LES ($\mathcal{F}^{step}$) fine grid simulations: (a) wall-normal location $y^+ = 11$, RANS-dominated region for all blending functions; (b) wall-normal location $y^+ = 100$, RANS-dominated region for $\mathcal{F}3$ and $\mathcal{F}4$ functions. Here the y-axis is shifted to show all the plots.

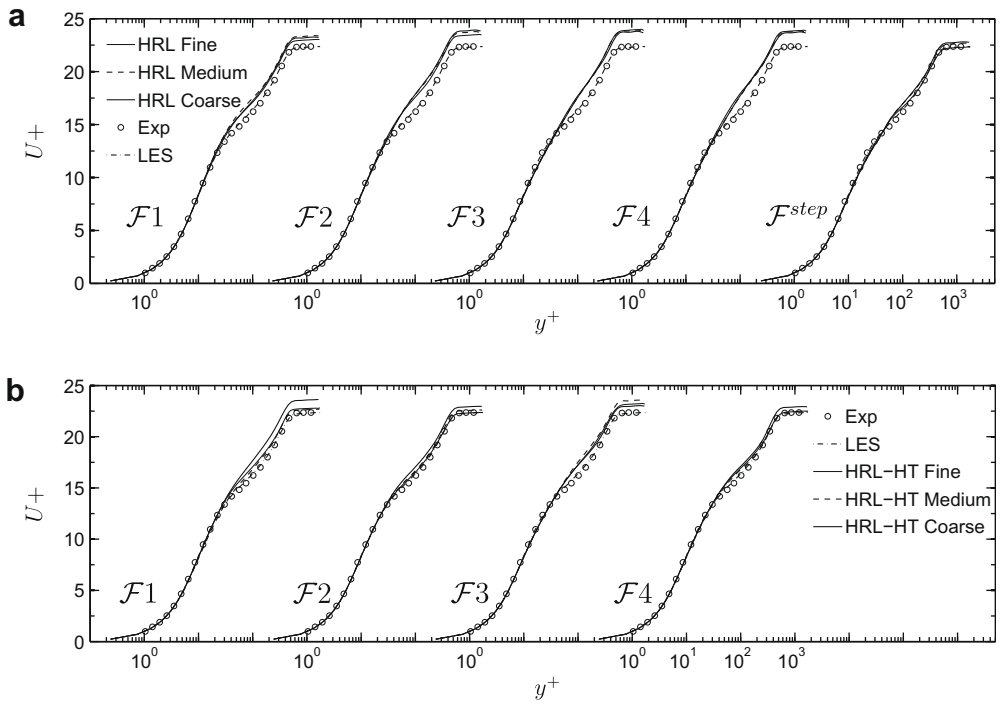

Fig. 10. Grid sensitivity studies, mean streamwise velocity profile U^+, for hybrid and Zonal RANS/LES ($\mathcal{F}^{step}$) simulations conducted on fine, medium, and coarse grids: (a) hybrid simulations not including the hybrid terms and (b) hybrid simulations including the hybrid terms.

outer layer $y^+ = 100$. As indicated by Fig. 3 and corroborated by Figs. 7–9, for all simulations, the intensity in the fluctuations are higher at $y^+ = 11$ than at $y^+ = 100$ for the streamwise velocity, while they are higher at $y^+ = 100$ than at $y^+ = 11$ for the spanwise and wall-normal velocities. However, in all simulations, the wavelengths of the fluctuations are smaller at $y^+ = 11$ than at $y^+ = 100$ indicating the presence of finer structures at the buffer layer. Overall, Figs. 7–9 demonstrate that the dissipation of the turbulent scales, due to RANS modeling, depends on the blending function implemented. At $y^+ = 11$, the highest reduction in velocity fluctuations, yet not complete dissipation, is obtained with the functions that set RANS modeling at the inner layer $\mathcal{F}2$, $\mathcal{F}3$, $\mathcal{F}4$, and $\mathcal{F}^{step}$, whereas $\mathcal{F}1$ simulations predict unsteady structures close to those of LES. This, strengthen the observation that the turbulent scales, fed in the RANS region by LES, are significantly reduced but are not dissipated entirely by RANS. In the other hand, as the hybrid formulation becomes more dominated by LES, the hybrid simulations resolve more unsteady turbulent content as seen in all velocity fluctuations at $y^+ = 100$. Figs. 7–9 also indicates that including the hybrid contributions has a positive effect in the unsteady velocities, which are slightly enhanced when the hybrid terms are included, due to their unsteady nature as indicated by Eqs. (2.53)–(2.58).

Thus far, the importance of the hybrid formulation has been demonstrated in a grid fine enough to conduct both LES (wall-resolving) and RANS simulations (solutions are grid independent). Nevertheless, it is pertinent to illustrate, up to some extent, the behavior of the hybrid formulation when none-wall resolving LES grids are implemented. Due to limited computational resources only the medium and coarse grids are evaluated with all the blending functions, while the coarsest grid is evaluated only with the $\mathcal{F}^{step}$ and $\mathcal{F}2$ functions which are selected to illustrate the effect of discontinuous and continuous functions with RTLT zone in the outer layer.

Fig. 10 presents the mean velocity profile computed with all blending functions using the fine, medium, and coarse grids. The figure indicates that for the blending function with RTLT zone close to the inner-layer, $\mathcal{F}1$, coarsening the grid to none-wall resolving resolutions, coarse grid, has a negative impact on the mean velocity profile even when the hybrid terms are included. Since the hybrid model is quickly dominated by LES at the near-wall region where the grid does not allow LES to resolve the near-wall dynamics. However, when the RTLT zone is in the outer layer, RANS dominates the hybrid formulation at the near-wall region, thus the effect of reducing the grid resolution is not as negative as in the previous case, as long as the hybrid terms are included. When these terms are included, the predicted velocity profiles do not change drastically even with the coarse grid. In the contrary, if the hybrid terms are neglected, a drop in accuracy in the predicted mean profile is observed for all blending functions. For the zonal RANS/LES simulation, $\mathcal{F}^{step}$, the medium and coarse grids predict results in close agreement to those obtained in the fine grid, mainly because the near-wall zone is completely modeled with RANS for this function. However, the velocity profiles still present similar discontinuities (results not shown) as those shown in Fig. 2(b).

The resolved, modeled, and total Reynolds stress $u'v'$, are shown in Figs. 11–13, respectively. The figures demonstrate that, for all blending functions with and without hybrid contributions, coarsening the grid tends to slightly increase and

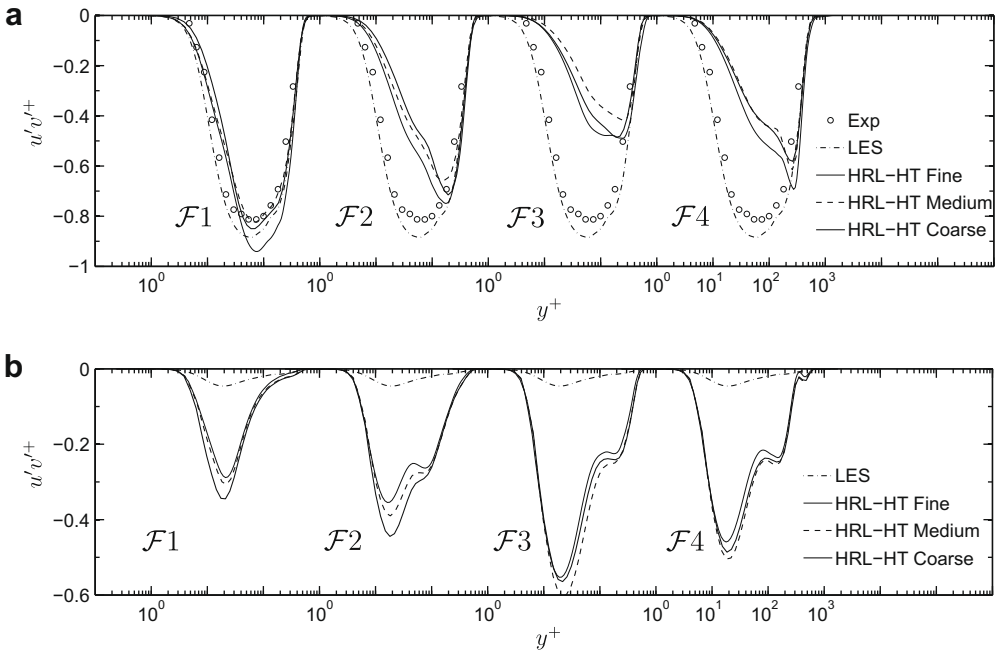

Fig. 11. Grid sensitivity studies for hybrid simulations including the hybrid terms conducted on fine, medium, and coarse grids: (a) resolved $u'v'^+$ Reynolds stress and (b) modeled $u'v'^+$ Reynolds stress.

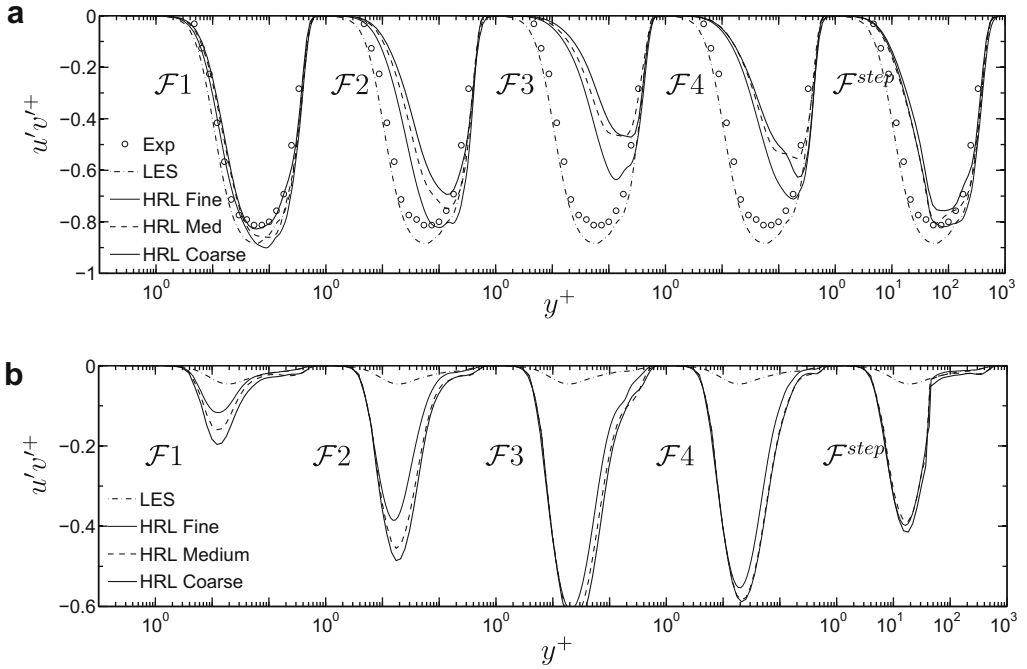

Fig. 12. Grid sensitivity studies for hybrid simulations not including the hybrid terms conducted on fine, medium, and coarse grids: (a) resolved $u'v'^{+}$ Reynolds stress and (b) modeled $u'v'^{+}$ Reynolds stress.

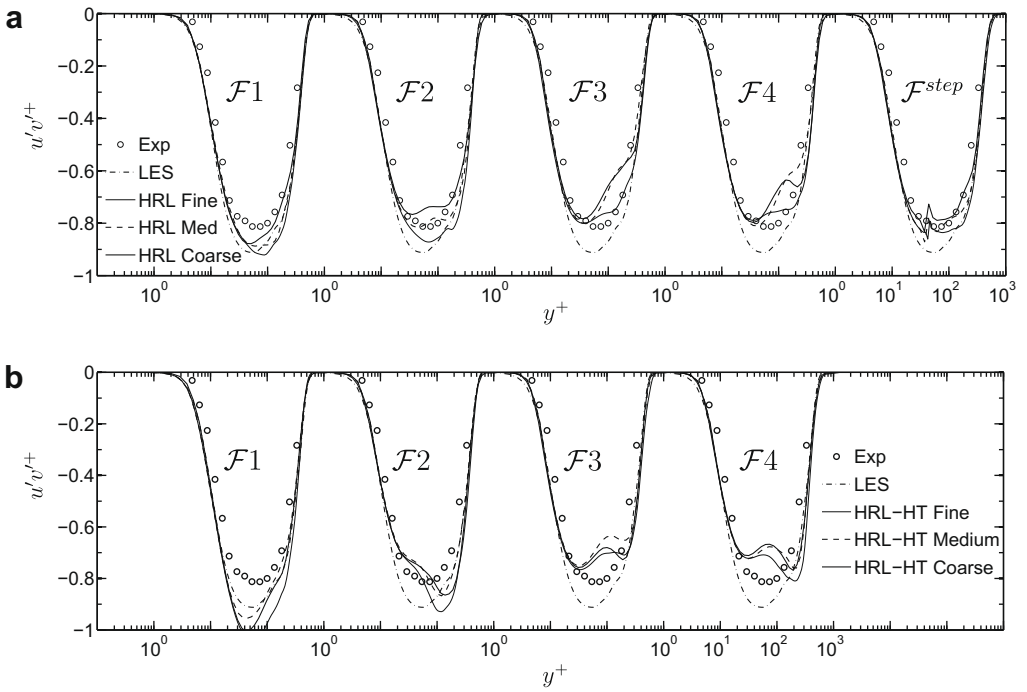

Fig. 13. Grid sensitivity studies, total $u'v'^{+}$ Reynolds stress (modeled plus resolved), for HRL, HRL-HT, and Zonal RANS/LES ($\mathcal{F}^{step}$) simulations conducted on fine, medium, and coarse grids: (a) hybrid simulations not including the hybrid terms and (b) hybrid simulations including the hybrid terms.

decrease the modeled and resolved stresses, respectively. However, the net effect in the total Reynolds stress is not very significant. Here, the zonal RANS/LES approach $\mathcal{F}^{step}$ is the less sensible to the reduction in grid resolution.

Overall, results obtained with all blending functions in the medium and coarse grids are quite good when the hybrid terms are included. This responds to the fact that those grids are still fine for hybrid simulations, i.e. the near-wall grid

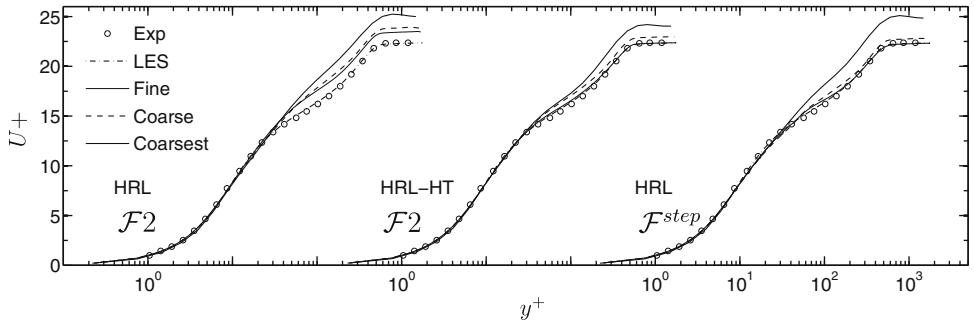

Fig. 14. Grid sensitivity studies, mean streamwise velocity profile U^+, for hybrid ($\mathcal{F}2$) and Zonal RANS/LES ($\mathcal{F}^{step}$) simulations conducted on fine, coarse, and coarsest grids.

resolution is good for RANS modeling and the outer-layer resolution is fine enough for LES. However, if we further reduce the grid resolution to levels not appropriated for LES, yet good for RANS, the predictions start to present significant anomalies. Fig. 14 presents the computed mean velocity profile using the fine, coarse, and coarsest grids with the $\mathcal{F}2$ and $\mathcal{F}^{step}$ blending functions. From the results is clear that the coarsest grid is not adequate for LES and consequently hybrid simulations, as

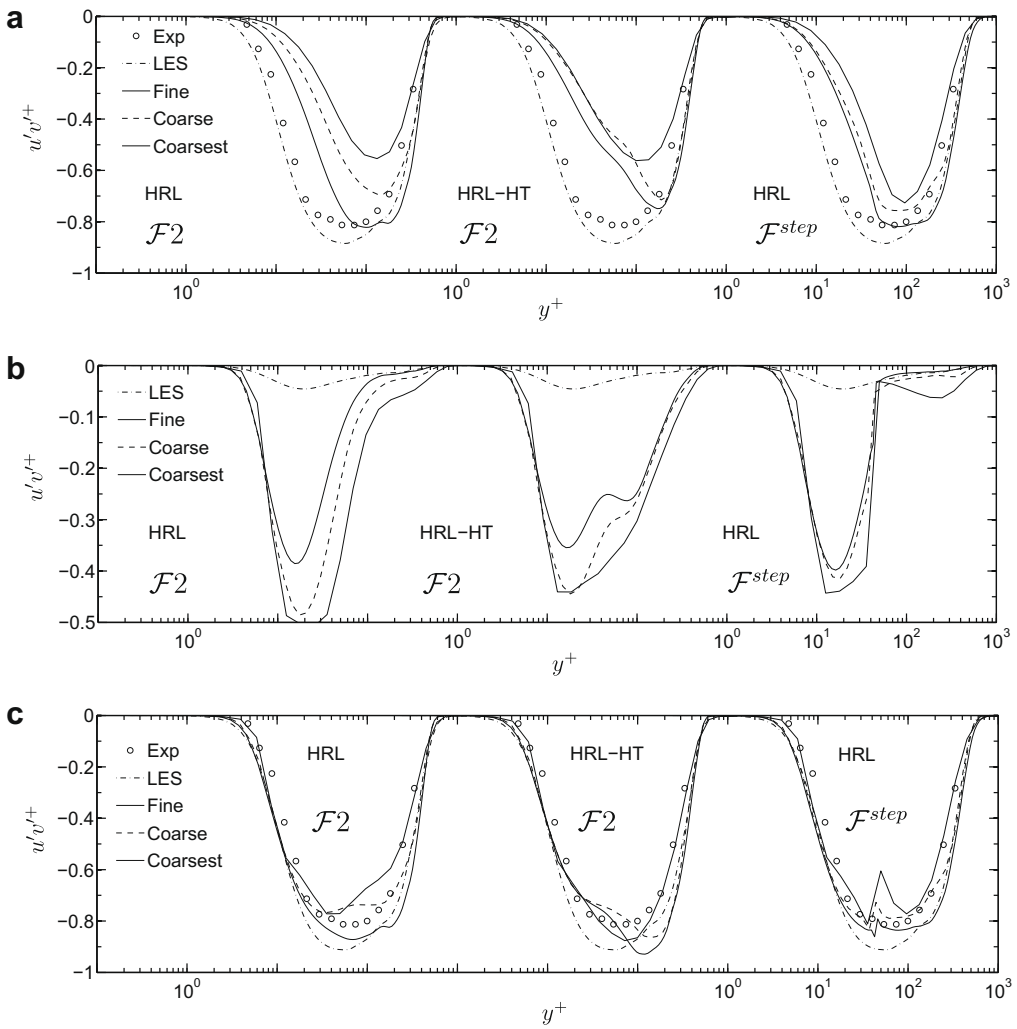

Fig. 15. Grid sensitivity studies for hybrid ($\mathcal{F}2$) and Zonal RANS/LES ($\mathcal{F}^{step}$) simulations conducted on fine, coarse, and coarsest grids: (a) resolved $u'v'^+$ Reynolds stress; (b) modeled $u'v'^+$ Reynolds stress; and (c) total (modeled plus resolved) $u'v'^+$ Reynolds stress.

demonstrated by the significant deviations predicted in the velocity profiles. However, by including the hybrid terms the mean velocity profile is slightly improved, demonstrating once more that Eqs. (2.41)–(2.46) have a positive effect in the hybrid formulation.

Fig. 15(a) and (b) presents the resolved and modeled Reynolds stress $u'v'$, it shows a drastic drop in the resolved stress and an important increase in the modeled stress for the $\mathcal{F}2$ function with respect to the fine and coarse grid results, specially when the hybrid terms are neglected. The increase in modeled stress at the RTLT zone is induced by the modeled stress coming from LES, which increases as the grid resolution decreases. In the other hand, for the zonal RANS/LES simulation the modeled stress, which is purely RANS below $y^+ = 45$, is virtually grid independent. However, in the LES region the resolved and modeled stresses drop and increase, respectively, due to the low grid resolution attained in the outer-layer.

The computed total stress shown in Fig. 15(c), shows an important droop at the RTLT zone when the hybrid contributions are neglected. This occurs because the grid is not fine enough there to resolve the turbulence and the modeled stresses drops because the hybrid terms are not included. However, when Eqs. (2.41)–(2.46) are included, fair agreement is reproduced with respect to the fine and coarse grids results, demonstrating once more the importance of the hybrid terms in this RANS/LES approach. The figure, also indicates that the discontinuities reproduced with the zonal RANS/LES approach are dramatically amplified when the grid resolution is significantly reduced, proving that zonal RANS/LES approaches will always predict nonphysical results and thus this approach should be avoided.

The approximated cost of the simulations (required to obtain statistics for a nondimensional time of $t_{aver}u_\tau^2/\nu_{wall} \sim 1800$ using the fine grid) given in single-processor hours on a Cray XT3 machine are the following: (a) Simulation 1 required around 6800 h, (b) simulations 2–6 required around 13,000 h, and (c) simulations 7–10 required around 15,000 h. Here, the cost of the hybrid simulations is about twice the cost of the LES simulations because each HRL-HT simulation runs simultaneously a LES simulation to provide the turbulent inflow and to explicitly compute the hybrid terms. If an effective closure model can be devised for the hybrid terms, since it is very likely that these terms cannot be computed directly from the hybrid field for general flows, then this cost can be drastically reduced.

4. Conclusion

In this paper, the compressible hybrid RANS/LES N–S equations are formally derived by applying a hybrid additive filter to the governing equations. The exact hybrid equations contain additional terms which importance is demonstrated in flat-plate turbulent boundary layer simulations. It is shown that the hybrid contributions, computed a priori from a LES simulation, helps to maintain the balance between the modeled and the resolved turbulence as the hybrid model transits from RANS to LES. An important observation, for attached flows, is that the hybrid RANS/LES simulations are not very sensitive to the hybrid blending function, as long as the hybrid contributions are included and the RTLT zone is located in the outer layer. However, if these terms are neglected, the accuracy of the simulations strongly depends on the blending function implemented. Additionally, it was demonstrated that under this hybrid formulation, the zonal RANS/LES approach, obtained by using a step function in the hybrid filter, predicts nonphysical discontinuities in the flow statistics. Further more, these anomalies are drastically amplified when the grid resolution is reduced. Consequently this approach should be avoided. Current results indicate that these unphysical discontinuities can be eliminated by using continuous blending functions together with the hybrid contributions.

Finally, based on the results here shown, further studies are required to prove that the hybrid terms are also important in more complex flows, specially when massive flow separation controls the flow dynamics. Additionally, further efforts have to be directed to develop simplified models for the hybrid contributions to make possible the application of the complete hybrid RANS/LES formulation in complex flows for engineering applications, without having to use the zonal RANS/LES approach or defining ad hoc transitions criteria between RANS and LES.

Acknowledgments

This work was sponsored in part by the National Rotorcraft Technology Center (NTRC) at the Georgia Institute of Technology, by NASA, by Army Research Office, and the Office of Naval Research. The computer resources of the Department of Defense Major Shared Resource Centers (MSRC) are gratefully acknowledged. The first author would also like to thank the National Council of Science and Technology of México (CONACYT).

Appendix. Incompressible hybrid Navier–Stokes equations

Although the incompressible hybrid RANS/LES N–S equations for an additive hybrid operator were first presented by Germano [39], these equations are repeated and expanded here to highlight the hybrid contributions, and to establish our new notation. The incompressible formulation is derived from the compressible hybrid approach (described in Section 2) by assuming incompressibility and by eliminating the energy and the state equations.

$$\frac{\partial \bar{u}_j}{\partial x_j} = \frac{\partial \mathcal{F}}{\partial x_j}[\dot{\bar{u}}_j - \ddot{\bar{u}}_j], \tag{A.1}$$

$$\begin{aligned}&\frac{\partial \bar{u}_i}{\partial t} + \bar{u}_j \frac{\partial \bar{u}_i}{\partial x_j} + \frac{\partial}{\partial x_j}(\bar{p}/\rho\delta_{ij} - \bar{\tau}_{ij}/\rho + \bar{\tau}(u_i,u_j)/\rho) \\ &\quad = \frac{\partial \mathcal{F}}{\partial x_j}[\dot{\bar{u}}_i\dot{\bar{u}}_j - \ddot{\bar{u}}_i\ddot{\bar{u}}_j + \dot{\bar{\tau}}(u_i,u_j)/\rho - \ddot{\bar{\tau}}(u_i,u_j)/\rho + (\dot{\bar{p}} - \ddot{\bar{p}})/\rho\delta_{ij} - (\dot{\bar{\tau}}_{ij} - \ddot{\bar{\tau}}_{ij})/\rho] \\ &\qquad - \nu\frac{\partial}{\partial x_j}\left\{\frac{\partial \mathcal{F}}{\partial x_j}(\dot{\bar{u}}_i - \ddot{\bar{u}}_i) + \frac{\partial \mathcal{F}}{\partial x_i}(\dot{\bar{u}}_j - \ddot{\bar{u}}_j)\right\} + \frac{\partial \mathcal{F}}{\partial t}[\dot{\bar{u}}_i - \ddot{\bar{u}}_i],\end{aligned} \tag{A.2}$$

$$\bar{\tau}_{ij} = \mu\left(\frac{\partial \bar{u}_i}{\partial x_j} + \frac{\partial \bar{u}_j}{\partial x_i}\right), \quad \dot{\bar{\tau}}_{ij} = \mu\left(\frac{\partial \dot{\bar{u}}_i}{\partial x_j} + \frac{\partial \dot{\bar{u}}_j}{\partial x_i}\right), \quad \ddot{\bar{\tau}}_{ij} = \mu\left(\frac{\partial \ddot{\bar{u}}_i}{\partial x_j} + \frac{\partial \ddot{\bar{u}}_j}{\partial x_i}\right), \tag{A.3}$$

$$\dot{\bar{\tau}}(a,b) = \rho(\dot{\overline{ab}} - \dot{\bar{a}}\dot{\bar{b}}), \tag{A.4}$$

$$\ddot{\bar{\tau}}(a,b) = \rho(\ddot{\overline{ab}} - \ddot{\bar{a}}\ddot{\bar{b}}), \tag{A.5}$$

$$\bar{\tau}(a,b) = \rho(\overline{ab} - \bar{a}\bar{b}). \tag{A.6}$$

Eqs. A.1,A.2 and A.6 represent the incompressible hybrid N–S equations and the hybrid second-order central-moment. The explicit expression for the hybrid central-moment is obtained by substituting Eq. (2.12) in Eq. (A.6),

$$\bar{\tau}(a,b) = \mathcal{F}\dot{\bar{\tau}}(a,b) + (1-\mathcal{F})\ddot{\bar{\tau}}(a,b) + \rho\mathcal{F}(1-\mathcal{F})(\dot{\bar{a}} - \ddot{\bar{a}})(\dot{\bar{b}} - \ddot{\bar{b}}) \tag{A.7}$$

and by operating Eq. (A.7) in u_i and u_j, the hybrid Reynolds stress tensor is directly obtained as

$$\bar{\tau}(u_i,u_j) = \rho[\mathcal{F}(\dot{\overline{u_iu_j}} - \dot{\bar{u}}_i\dot{\bar{u}}_j) + (1-\mathcal{F})(\ddot{\overline{u_iu_j}} - \ddot{\bar{u}}_i\ddot{\bar{u}}_j) + \mathcal{F}(1-\mathcal{F})(\dot{\bar{u}}_i - \ddot{\bar{u}}_i)(\dot{\bar{u}}_j - \ddot{\bar{u}}_j)]. \tag{A.8}$$

The momentum equation derived here is slightly different from Germano's original derivation since we keep the definition for the viscous stress tensor (A.3) while Germano applied continuity to simplify the momentum equation. Nevertheless, it can be shown that both equations are consistent.

Finally, by substituting Eqs. (A.4) and (A.5) in Eq. (A.2), and the differences between RANS and LES variables with the turbulence fluctuations ($\dot{\phi'} = \phi - \dot{\bar{\phi}} = \mathcal{C}(\ddot{\bar{\phi}} - \dot{\bar{\phi}})$, with $\mathcal{C} = 1$) it can be shown that the hybrid contributions take the following form:

$$\sigma_\rho = -\frac{\partial \mathcal{F}}{\partial x_j}\dot{u_j'}, \tag{A.9}$$

$$\sigma_{\rho u_i} = -\frac{\partial \mathcal{F}}{\partial x_j}[(u_iu_j)\dot{'} + \dot{p'}/\rho\delta_{ij} - \dot{\tau_{ij}'}/\rho] + \nu\frac{\partial}{\partial x_j}\left\{\frac{\partial \mathcal{F}}{\partial x_j}\dot{u_i'} + \frac{\partial \mathcal{F}}{\partial x_i}\dot{u_j'}\right\} - \frac{\partial \mathcal{F}}{\partial t}\dot{u_i'} \tag{A.10}$$

$$\sigma_{\bar{\tau}(u_i,u_j)} = \rho\mathcal{F}(1-\mathcal{F})\dot{u_i'}\dot{u_j'} \tag{A.11}$$

Similar to the compressible formulation, the incompressible hybrid contributions represent turbulence scales and need to be included.

References

[1] P.R. Spalart, Strategies for turbulence modelling and simulations, Int. J. Heat Fluid Flow 21 (2000) 252–263.
[2] U. Piomelli, E. Balaras, Wall-layer models for large-eddy simulations, Annu. Rev. Fluid Mech. 34 (2002) 349–374.
[3] U. Schumann, Subgrid scale model for finite difference simulations in plane channels and annuli, J. Comput. Phys. 18 (1975) 376.
[4] P.R. Spalart, W.H. Jou, M. Strelets, S.R. Allmaras, Comments on the feasibility of LES for wings and on a hybrid RANS/LES approach, in: First AFOSR International Conference on DNS/LES, Ruston Louisiana, 4–8 August 1997, Greyden Press.
[5] C.G. Speziale, Turbulence modeling for time dependent RANS and VLES: a review, AIAA J. 36 (2) (1998) 173–184.
[6] P. R Spalart, S.R. Allmaras, A one-equation turbulence model for aerodynamic flows, La Recherche Aerospatiale 1 (1994) 5–21.
[7] M. Strelets, Detached eddy simulation of massively separated flows, AIAA Paper 01-0879, 8–11 January 2001.
[8] U. Piomelli, E. Balaras, H. Pasinato, K.D. Squires, P.R. Spalart, The inner-outer layer interface in large-eddy simulations with wall-layer models, Int. J. Heat Fluid Flow 24 (2003) 538–550.
[9] K.D. Squires, Detached-eddy simulation: current status and perspectives, in: R. Friedrich, B.J. Geurts, O. Metais (Eds.), Direct and Large Eddy simulation, vol. V, Kluwer, Dordrecht, 2004, pp. 465–480.
[10] A.K. Viswanathan, D.K. Tafti, Detached eddy simulation of flow and heat transfer in fully developed rotating internal cooling channel with normal ribs, Int. J. Heat Fluid Flow 27 (2006) 351–370.
[11] A. Keating, U. Piomelli, A dynamic stochastic forcing method as a wall-layer model for large-eddy simulation, J. Turbul. 7 (12) (2006).
[12] H. Paik, C. Escauriaza, F. Sotiropoulos, On the bimodal dynamics of the turbulent horseshoe vortex system in a wing-body junction, Phys. Fluids 19 (2007) 045107–045120.
[13] N.V. Nikitin, F. Nicoud, B. Wasistho, K.D. Squires, P.R. Spalart, An approach to wall modeling in large-eddy simulations, Phys. Fluids 12 (2000) 1629–1632.
[14] P.R. Spalart, Young person's guide to detached-eddy simulation grids, NASA CR-2001 211032, 2001.
[15] P.R. Spalart, S. Deck, M.L. Shur, K.D. Squires, M.Kh. Strelets, A. Travin, A new version of detached-eddy simulation resistant to ambiguous grid densities, Theor. Comput. Fluid Dyn. 20 (2006) 181–195.
[16] P. Batten, U. Goldberg, S. Chakravarthy, Interfacing statistical turbulence closures with large-eddy simulation, AIAA J. 42 (3) (2004) 485–492.
[17] N.S. Liu, T.H. Shih, Turbulence modeling for very large-eddy simulation, AIAA J. 44 (4) (2006) 687–697.
[18] C. Delanghe, B. Merci, E. Dick, Hybrid RANS/LES modelling with an approximate renormalization group. I: Model development, J. Turbul. 6 (13) (2005).

[19] S.S. Girimaji, Partially-averaged Navier–Stokes model for turbulence: a Reynolds-averaged Navier–Stokes to direct numerical simulation bridging method, J. Appl. Mech.–Trans. ASME 73 (2006) 413–421.
[20] I. Befeno, R. Schiestel, Non-equilibrium mixing of turbulence scales using a continuous hybrid RANS/LES approach: application to the shearless mixing layer, Flow Turbul. Combust. 78 (2007) 129–151.
[21] N.J. Georgiadis, J.I.D. Alexander, E. Reshotko, Hybrid Reynolds-averaged Navier–Stokes/large-eddy simulations of supersonic turbulent mixing, AIAA J. 41 (2) (2003) 218–229.
[22] F. Hamba, A hybrid RANS/LES simulation of turbulent channel flow, Theor. Comput. Fluid Dyn. 16 (2003) 387–403.
[23] P. Tucker, L. Davidson, Zonal $k - l$ based large eddy simulation, Comput. Fluids 33 (2) (2004) 267–287.
[24] J.U. Schluter, H. Pitsch, P. Moin, Large eddy simulation inflow conditions for coupling with Reynolds-average flow solvers, AIAA J. 42 (3) (2004) 478–484.
[25] B. Zhong, P.G. Tucker, $k - l$ based hybrid LES/RANS approach and its applications to heat transfer simulation, Int. J. Numer. Meth. Fluids 46 (2004) 983–1005.
[26] L. Davidson, S. Dahlström, Hybrid LES-RANS: an approach to make LES applicable at high Reynolds number, Int. J. Comput. Fluid Dyn. 19 (6) (2005) 415–427.
[27] L. Temmerman, M. Hadziabdic, M.A. Leschziner, K. Hanjalic, A hybrid two-layer URANS-LES approach for large eddy simulation at high Reynolds number, Int. J. Heat Fluid Flow 26 (2005) 173–190.
[28] L. Davidson, M. Billson, Hybrid LES–RANS using synthesized turbulent fluctuations for forcing in the interface region, Int. J. Heat Fluid Flow 27 (2006) 1028–1042.
[29] F. Hamba, A hybrid RANS/LES simulation of high-Reynolds-number channel flow using additional filtering at the interface, Theor. Comput. Fluid Dyn. 20 (2) (2006) 89–101.
[30] J.S. Baggett, On the feasibility of merging LES with RANS for the near wall region of attached turbulent flows, in; Annual Research Briefs, Center for Turbulence Research, 1998, pp. 267–277.
[31] X. Xiao, J.R. Edwards, H.A. Hassan, R.A. Baurle, Inflow boundary conditions for hybrid large eddy/Reynolds Averaged Navier–Stokes simulations, AIAA J. 41 (8) (2003) 1481–1489.
[32] R.A. Baurle, C.J. Tam, J.R. Edwards, H.A. Hassan, Hybrid simulation approach for cavity flows: blending, algorithm, and boundary treatment issues, AIAA J. 41 (8) (2003) 1463–1480.
[33] X. Xiao, J.R. Edwards, H.A. Hassan, Blending functions in hybrid large-eddy/Reynolds-averaged Navier–Stokes simulations, AIAA J. 42 (12) (2004) 2508–2515.
[34] C.-C. Fan, X. Xiao, J.R. Edwards, H.A. Hassan, R.A. Baurle, Hybrid large-eddy/Reynolds-averaged Navier–Stokes simulations of shock-separated flows, J. Spacecr. Rockets 41 (6) (2004) 897–906.
[35] S. Kawai, K. Fujii, Analysis and prediction of thin-airfoil stall phenomena with hybrid turbulence methodology, AIAA J. 43 (5) (2005) 953–961.
[36] L. Davidson, S.H. Peng, Hybrid LES–RANS modelling: a one-equation sgs model combined with a $k - \omega$ model for predicting recirculating flows, Int. J. Numer. Meth. Fluids 43 (2003) 1003–1018.
[37] J. Smagorinsky, General circulation experiments with the primitive equations: I. The basic equations, Monthly Weather Rev. 91 (1963).
[38] E. Labourasse, P. Sagaut, Reconstruction of turbulent fluctuations using a hybrid RANS/LES approach, J. Comput. Phys. 182 (2002) 301–336.
[39] M. Germano, Properties of the hybrid RANS/LES filter, Theor. Comput. Fluid Dyn. 17 (2004) 225–231.
[40] P. Sagaut, Large Eddy Simulation for Incompressible Flows, An Introduction, third ed., Springer, 2005.
[41] S. Heinz, Unified turbulence models for LES and RANS FDF and PDF simulations, Theor. Comput. Fluid Dyn. 21 (2007) 99–118.
[42] K. Hanjalic, Will RANS survive LES a view of perspectives, J. Fluids Eng.-Trans. ASME 127 (5) (2005) 831–839.
[43] A.S. Monin, A.M. Yaglom, Statistical Fluid Mechanics, MIT Press, 1979.
[44] M. Germano, Turbulence: the filtering approach, J. Fluid Mech. 238 (1992) 325–336.
[45] E.F. Spina, A.J. Smits, S.K. Robinson, The physics of supersonic turbulent boundary layers, Annu. Rev. Fluid Mech. 26 (1994) 287–319.
[46] D.C. Wilcox, Reassessment of the scale-determining equation for advanced turbulence models, AIAA J. 26 (11) (1998) 1299–1310.
[47] S. Menon, N. Patel, Subgrid modeling for simulation of spray combustion in large-scale combustors, AIAA J. 44 (4) (2006) 709–723.
[48] F.R. Menter, Two-equation eddy-viscosity turbulence models for engineering applications, AIAA J. 32 (8) (1994) 1598–1605.
[49] D.B. DeGraaff, J.K. Eaton, Reynolds-number scaling of the flat-plate turbulent boundary layer, J. Fluid Mech. 422 (2000) 319–346.
[50] A. Jameson, Time dependent calculations using multigrid, with applications to unsteady flows past airfoils and wings, AIAA Paper 91-1596, January 1991.
[51] F. Ducros, F. Laporte, T. Souleres, V. Guinot, P. Moinat, B. Caruelle, High-order fluxes for conservative skew-symmetric-like schemes in structured meshes: application to compressible flows, J. Comput. Phys. 161 (2000) 114–139.
[52] D.V. Gaitonde, M.R. Visbal, Pade-type higher-order boundary filters for the Navier–Stokes equations, AIAA J. 38 (11) (2002) 2103–2112.
[53] C. Hirsch, Numerical Computation of Internal and External Flows Computational Methods for Inviscid and Viscous Flows, Wiley, 1990.
[54] T.S. Lund, X. Wu, K.D. Squires, Generation of turbulent inflow data for spatially-developing boundary layer simulations, J. Comput. Phys. 140 (1998) 233–258.
[55] A. Ferrante, S.E. Elghobashi, A robust method for generating inflow conditions for direct simulations of spatially-developing turbulent boundary layers, J. Comput. Phys. 198 (2004) 372–387.
[56] J.F. Thompson, B. K Soni, N.P. Weatherill, Handbook of Grid Generation, CRC Press, 1998.